Role of Reelin in cell positioning in the cerebellum and the cerebellum-like structure in zebrafish

Takayuki Nimura[1], Tsubasa Itoh[1], Hanako Hagio[1,2], Takuto Hayashi[1], Vincenzo Di Donato[3,†], Miki Takeuchi[4], Takeaki Itoh[5], Fuduki Inoguchi[5], Yoshikatsu Sato[6], Naoyuki Yamamoto[2], Yu Katsuyama[5], Filippo Del Bene[3], Takashi Shimizu[1,4], and Masahiko Hibi[1,4,§]

[1]Division of Biological Science, Graduate School of Science, Nagoya University, Furo, Chikusa, Nagoya, Aichi 464-8602, Japan
[2]Department of Animal Sciences, Graduate School of Bioagricultural Sciences, Nagoya University, Nagoya, Aichi 464-8601, Japan
[3]Institut Curie, PSL Research University, INSERM U934, CNRS UMR3215, UPMC Paris-Sorbonne, Paris 75005, France
[4]Bioscience and Biotechnology Center, Nagoya University, Furo, Chikusa, Nagoya, Aichi 464-8601, Japan
[5]Department of Anatomy, Shiga University of Medical Science, Otsu, Shiga 520-2912, Japan
[6]Institute of Transformative Bio-Molecules, Nagoya University, Furo, Chikusa, Nagoya, Aichi 464-8601, Japan

[†]Present address: ZeClinics SL, Barcelona Biomedical Research Park (PRBB), Barcelona 08003, Spain
[§]Author for correspondence (hibi@bio.nagoya-u.ac.jp)

Running Head: Reelin for the cerebellum and the cerebellum-like structure
Key words: Reelin, cerebellum, cerebellum-like structure, mesencephalic tectum, layer formation, neural circuit formation, axonal transport, zebrafish

ABSTRACT

The cerebellum and the cerebellum-like structure in the mesencephalic tectum in zebrafish contain multiple cell types, including principal cells (i.e., Purkinje cells and type I neurons) and granule cells, that form neural circuits in which the principal cells receive and integrate inputs from granule cells and other neurons. It is largely unknown how these cells are positioned and how neural circuits form. While Reelin signaling is known to play an important role in cell positioning in the mammalian brain, its role in the formation of other vertebrate brains remains elusive. Here we found that zebrafish with mutations in Reelin or in the Reelin-signaling molecules Vldlr or Dab1a exhibited ectopic Purkinje cells, eurydendroid cells (projection neurons), and Bergmann glial cells in the cerebellum, and ectopic type I neurons in the tectum. The ectopic Purkinje cells and type I neurons received aberrant afferent fibers in these mutants. In wild-type zebrafish, *reelin* transcripts were detected in the internal granule cell layer, while Reelin protein was localized to the superficial layer of the cerebellum and the tectum. Laser ablation of the granule cell axons perturbed the localization of Reelin, and the mutation of both *kif5aa* and *kif5ba*, which encode major kinesin I components in the granule cells, disrupted the elongation of granule cell axons and the Reelin distribution. Our findings suggest that in zebrafish, (1) Reelin is transported from the granule cell soma to the superficial layer by axonal transport; (2) Reelin controls the migration of neurons and glial cells from the ventricular zone; and (3) Purkinje cells and type I neurons attract afferent axons during the formation of the cerebellum and the cerebellum-like structure.

1. Introduction

The precise positioning of neurons and glial cells is a prerequisite for the formation of functional neural circuits in animals. *Reelin* (*Reln*), the responsible gene for the *reeler* mouse, plays important roles in cell positioning and layer formation in the mammalian brain. The *reeler* mouse was originally described as a mutant with behavioral phenotypes characterized by ataxia and a reeling gate (Falconer, 1951). Later, *Reln* was identified, and its product, Reln protein was found to consist of eight unique repeats (reelin repeats), each of which contains an epidermal growth factor (EGF)-like cysteine pattern in its center (Suppl. Fig. 1) (D'Arcangelo et al., 1995). Reln binds to the cell surface receptors apolipoprotein E receptor 2 (ApoER2, also known as low-density lipoprotein receptor-related protein 8, LRP8) and very-low-density lipoprotein receptor (VLDLR), which are members of the low-density lipoprotein receptor family (D'Arcangelo et al., 1999; Hiesberger et al., 1999). Reln's binding to these receptors leads to phosphorylation of the intracellular adaptor protein, disabled 1 (Dab1), by Src-family tyrosine kinases Fyn and Src (Howell et al., 1999). ApoER2 and VLDLR-double mutant mice (Trommsdorff et al., 1999), Dab1 mutant mice (Kojima et al., 2000; Sheldon et al., 1997; Sweet et al., 1996; Ware et al., 1997; Yoneshima et al., 1997), Fyn/Src-double mutant mice (Kuo et al., 2005), and mice deficient in the tyrosine phosphorylation sites of Dab1 (Howell et al., 2000), all show *reeler*-like phenotypes, indicating that the Reln-ApoER2/VLDLR-Dab1 pathway is essential for Reln-mediated cell positioning and layer formation.

The roles of Reln in neural development have been well investigated with respect to layer formation of the mammalian neocortex. The neocortex has six layers, in which early-born neurons are located in the deep layers, whereas later-born neurons are located in the superficial layers (called an “inside-out” pattern). In *reeler* mutants, the cortical layers form abnormally (Boyle et al., 2011; Caviness, 1973; D'Arcangelo et al., 1995; Dekimoto et al., 2010; Hertel and Redies, 2011; Mikoshiba et al., 1980; Ogawa et al., 1995). This abnormal layer formation is attributed to the aberrant migration of cortical neurons [reviewed in (Hirota and Nakajima, 2017; Lee and D'Arcangelo, 2016; Sekine et al., 2014)]. Mouse mutants deficient in Reln (*reeler*) or Reln-signaling molecules also show abnormal layer formation and severe hypoplasia in the cerebellum. The mouse cerebellum has a molecular layer (ML), Purkinje cell layer (PCL), granule cell layer (GCL), and white matter (WM). The *reeler* mutants do not form the PCL properly, and many ectopic Purkinje cells are present in the GCL and intermingled with the WM (Heckroth et al., 1989; Mariani et al., 1977; Yuasa et al., 1993). In addition, Bergmann glial cells (BGs) are ectopically localized and their fibers are aberrantly oriented in these mutants (Terashima et al., 1985). The *reeler* mutants also exhibit a severely reduced number of granule cells (GCs), resulting in cerebellar hypoplasia (Terashima et al., 1985). In wild-type postnatal mice, Reln is expressed by GCs in the external granular cell layer (EGL) in the cerebellum primordium and in the internal GCL (D'Arcangelo et al., 1995; Miyata et al., 1996; Miyata et al., 2010; Schiffmann et al., 1997). Reln is thought to primarily control the migration of Purkinje cells (PCs), which are generated from neural progenitors in the ventricular zone (VZ).

Early/posterior-born PCs migrate tangentially from the VZ with a longer leading and shorter trailing process, and then change their orientation by sending their trailing process to the pial side to form the Purkinje plate (primordial PCL) beneath the EGL (Miyata et al., 2010). Anterior-born PCs migrate radially to reach the PCL; this migration is thought to be guided by radial glial fibers (Hatten and Heintz, 1995; Yuasa et al., 1991). The *reeler* mutants lack the orientation change of the early/posterior-born PCs near the Reln-rich EGL (Miyata et al., 2010), indicating that short-range Reln signaling plays a role in the initial arrangement of the PCL. Explant analysis suggested that Reln also functions as a long-range chemoattractant for PCs (Miyata et al., 1997). Expressing *Reln* in neural precursors under control of the *Nestin* promoter rescues the PCL formation in the *reeler* mutants (Magdaleno et al., 2002). These findings imply that multiple mechanisms are involved in PC migration. The *reeler* mouse and SRK (*Reln*-deficient) rat mutants also display abnormalities in cell positioning and layer formation in the superior colliculus of the mesencephalic tectum and aberrant projections of afferent fibers (retinotectal and corticotectal) to the optic tectum (Baba et al., 2007; Sakakibara et al., 2003). However, it is not clear what types of cells are mispositioned in the tectum of these mutants.

It also remains elusive how Reln signaling controls neural development in other vertebrate species. Comparative studies with Reln-signaling mutants in other vertebrate species could clarify the general role of Reln signaling in vertebrate neural development. The cerebellum is generally conserved between mammals and zebrafish (Hashimoto and Hibi, 2012; Hibi et al., 2017; Hibi and Shimizu, 2012). The anatomical

and developmental processes of the zebrafish cerebellum and the cerebellar neural circuits are well investigated; there are many molecular markers for specific components of the cerebellar neural circuits and transgenic fish in which such components are marked (Bae et al., 2009; Kani et al., 2010; Takeuchi et al., 2015a; Takeuchi et al., 2017; Wullimann et al., 2011) (Table 1). The zebrafish cerebellum contains GCs, PCs, and BGs like the mammalian cerebellum, and it additionally has eurydendroid cells (ECs), which are projection neurons that function similarly to the neurons in the deep cerebellar nuclei in mammals. The zebrafish cerebellum has a simple lobular structure (four domains: the valvula cerebelli, Va; corpus cerebelli, CCe; lobus caudalis, LCa; and eminentia granularis, EG) and three layers (the ML, PCL, and GCL, but not WM) (Hashimoto and Hibi, 2012; Hibi et al., 2017; Hibi and Shimizu, 2012) (Fig. 1A, B). The differentiation of GCs and PCs from their progenitors and their migration processes are similar in the zebrafish and mammalian cerebellum (Kani et al., 2010). These findings suggest that the zebrafish cerebellum would provide a good model for studying Reln-mediated cell positioning. As in other teleost species, the zebrafish has a cerebellum-like structure that contains GCs and principal cells (PC-like neurons) outside the cerebellum (Bell, 2002; Bell et al., 2008; Sawtell and Bell, 2008). In the cerebellum-like structure, the principal cells receive two types of inputs (afferent fibers) including GC axons, and integrate their information to generate output. In the mesencephalic tectum, which includes the optic tectum and the torus longitudinalis (TL), type I neurons function as the principal cells, and extend their dendrites superficially into the marginal layer (stratum marginale, SM), where they receive axons from GCs

located in the TL and the retina (Bell, 2002; Bell et al., 2008; Folgueira et al., 2007; Ito et al., 2003; Northmore, 2017; Wullimann, 1994) (Fig. 1A, C). The neurons in the cerebellum and the cerebellum-like structures express a similar set of genes (Bae et al., 2009; Katsuyama et al., 2007; Mikami et al., 2004; Takeuchi et al., 2017). However, it remains to be elucidated whether the same mechanisms control cell positioning and neural circuit formation in the cerebellum and cerebellum-like structure. Here we demonstrate that in zebrafish, Reln signaling is involved in the cell positioning of neurons in both the cerebellum and the cerebellum-like structure, and that axonal transport in GCs may play a role in the proper distribution of Reln.

2. Materials and methods

2.1. Ethics statement

The animal work in this study was approved by the Nagoya University Animal Experiment Committee and was conducted in accordance with the Regulations on Animal Experiments at Nagoya University

2.2. Zebrafish strains and husbandry

Wild-type zebrafish (*Danio rerio*) with the Oregon AB genetic background were used. The allele name of the *reln*$^{\Delta 7}$ mutant established in this study is designated *reln*^{nub23} in ZFIN (http://zfin.org). The *reln*$^{\Delta 28}$, *vldlr*$^{+13}$, and *dab1a*$^{\Delta 14}$ mutants were established

previously (Di Donato et al., 2018). We confirmed the sequence of all the mutant alleles (predicted protein structure of the mutant proteins is shown in Suppl. Fig. S1) The sequence of *vldlr*$^{+13}$ was slightly different from the published one, possibly due to an error in sequencing the mutant locus. The sequence of *dab1a*$^{\Delta 14}$ was also different from the previously published one (*dab1a*$^{\Delta 22}$). The *vldlr*$^{\Delta 9}$ and *dab1a*$^{\Delta 14}$ mutants were probably derived from *vldlr* and *dab1a* mutant populations that contained multiple alleles. The *kif5aa*^{*162} and *kif5ba*^{ae12} mutants were also described previously (Auer et al., 2015; Campbell et al., 2015). The transgenic zebrafish lines hspGFFDMC28C, hspzGFFgDMC156A, SAGFF(LF)251A, and hspGFFDMC90A, which express a modified version of Gal4-VP16 (GFF) in the inferior olivary nucleus (IO) neurons, the ECs, the BGs, and the GCs, respectively, were reported previously and crossed with a UAS:GFP line (nkuasgfp1aTg) to visualize these cells (Takeuchi et al., 2015a). *Tg(aldoca:gap43-Venus)* was used to visualize PCs (Takeuchi et al., 2015a; Tanabe et al., 2010). Zebrafish were maintained in environmentally controlled rooms at the Bioscience and Biotechnology Center, Nagoya University. Zebrafish embryos were reared as described previously (Westerfield, 2000). For immunohistochemistry and whole-mount in situ hybridization, larvae were treated with 0.003% phenylthiourea from 12 hours post-fertilization to prevent pigmentation. Adult fish were 90 days or older; juvenile fish were between 30 and 89 days old; and larvae were between 3 and 29 days old.

2.3. Generation of a reln mutant by CRISPR/Cas9, and the genotyping of mutants

A CRISPR/Cas9 target was selected in the zebrafish *reln* gene using the web software ZiFiT Targeter ver. 4.2 (http://zifit.partners.org/ZiFiT/) (Hwang et al., 2013; Mali et al., 2013). To generate gRNA, the oligonucleotides 5'-TAGGAGCAGGACGAGTGGGCGC-3' and 5'- AAACGCGCCCACTCGTCCTGCT-3' were annealed and subcloned into pT7-gRNA (Jao et al., 2013). The gRNA was synthesized from the *BamH*I-digested pT7-gRNA plasmid with T7 RNA polymerase (Promega). The Cas9 RNA was synthesized from pCS2+hSpCas9 (Ansai and Kinoshita, 2014), which contains the human codon-optimized *S. pyogens* Cas9 gene (Cong et al., 2013), in the presence of m'G(5')G RNA Cap Structure Analog (NEB). A solution containing 25 ng/μL gRNA and 100 ng/μL Cas9 RNA was injected into one-cell-stage embryos. To detect insertion and/or deletion (indel) mutations, the target regions were amplified and subjected to a heteroduplex mobility assay (HMA) (Ota et al., 2013). The target regions amplified from the mutant genome were subcloned into pTAC-2 (BioDynamics Laboratory Inc.), and the mutations were confirmed by sequencing. The following primers were used for genotyping: 5'- CGTTTCCGCTGGATCCAGA-3' and 5'-CGTGGCACATCTGTGGACA-3' to detect the *reln*$^{\Delta 7}$ mutation; 5'-TGCAGTAAGTCTGCGTCTGC-3' and 5'-TGTGTGTATGCGGAGCAGC-3' to detect the *reln*$^{\Delta 28}$ mutation; 5'-AGATGTCAACGAGTGCCTCA-3' and 5'-CACTCGCATTTGTATCCTCCT-3' to detect the *vldlr*$^{+13}$ mutation; 5'-GCAGTGAAGCAGCTCTGATAAA and 5'-TCCTCTAGCTGCAGTGACCTC-3' to detect the *dab1a*$^{\Delta 14}$ mutation; 5'-CGAGGACATCTTCAACCACATC-3' and 5'-GTGTACCTTGATGTGGAACTCC-3' to detect the *kif5aa*^{*162} mutation; and

5'-CTTTCAGGGACAGGATAGCG-3’ and 5'-ATTAGCATTAGCCGTTCGCG-3’ to detect the *kif5ba*$_{ae12}$ mutation. The PCR products were separated on 12% TBE (Tris-borate-EDTA) acrylamide gels or 1-2.5% TAE (Tris-acetate-EDTA) agarose gels.

2.4. In situ hybridization

In situ hybridization of larvae and sections was performed as described previously (Bae et al., 2009). The plasmids for a riboprobe of *reln* and a glutamate receptor, ionotropic delta2 interacting protein, a (*grid2ipa*) were described previously (Costagli et al., 2002; Takeuchi et al., 2017). A digoxigenin (DIG)-labeled riboprobe was made using SP6 or T7 RNA polymerase after restriction-enzyme digestion. Signals were detected with alkaline-phosphatase conjugated with anti-DIG Fab fragments (Roche) using NBT/BCIP (Roche) as a chromogenic substrate. NBT/BCIP signals were acquired using an AxioPlan-2 microscope equipped with an AxioCam CCD camera (Zeiss).

2.5. Immunostaining, imaging, and measurement

For immunostaining, anti-parvalbumin7 (Pvalb7, 1:1000, mouse ascites), anti-Vglut1 (1:1000, rabbit purified), anti-Neurod1 (1:500, mouse ascites) (Bae et al., 2009; Kani et al., 2010), anti-Reelin (1:500, MAB5366, rabbit Merck) (Di Donato et al., 2018), anti-calretinin (1:1000, rabbit, 7697, Swant), anti-GFP (1:1000, rat, 04404-84, Nacalai Tesque), and anti-glutamate receptor, ionotropic, delta2 (Grid2, 1:200, rabbit, GluRd2C(852-931)-Rb-Af500, Frontier Institute Co. Ltd) antibodies were used. CF™ 568 goat anti-mouse IgG [H+L] (1:400, 20301, Biotium), CF™ 488A goat anti-rabbit

IgG [H+L] (1:400, 200019, Biotium), and CF™ 488A goat anti-rat IgG [H+L] (1:400, 20023, Biotium) antibodies were used singly or in combination as secondary antibodies. Larvae and cryosections were immunostained as described previously (Bae et al., 2009), except that 14-μm sections were prepared by a cryostat. For Reelin immunostaining, sections were preincubated in 0.01 M sodium citrate for 30 min and in 1% SDS for 5 min. Some sections were co-stained with a cell nuclear marker Hoechst33342 (PA-3014, Lonza). Fluorescence images were obtained with an LSM700 confocal laser-scanning microscope or an Axioplan2 microscope/AxioCam CCD camera. The projection images were constructed from Z-stack sections using the 3D-projection program associated with the microscope (ZEN, Zeiss). The figures were constructed using Adobe Photoshop, Adobe Illustrator, and Microsoft PowerPoint. Brightness and contrast adjustments were applied equally to all digital images in each figure. GFP^+ (BG) areas in the GCL or the entire cerebellum were measured by Image J software (https://imageh.nih.gov/ij/) and its binarization program (see Fig. 5). Distance between the pia and neurons (type I neurons) was determined from the Axoplan2 images by AxioVision (Zeiss) (see Fig. 6). The length and thickness of $Vglut1^+$ or $Reln^+$ regions were determined using Image J software.

2.6. Tracing of type I neurons

We injected biotinylated dextran amine (BDA: molecular weight 3000; D7135; Molecular Probe) into the stratum marginale (SM) of the optic tectum. Fish were anesthetized by immersing in fresh water containing 180 mg/L tricaine

methanesulfonate (MS222; Sigma) and set in a device for physical restraint. The fish were aerated with fresh water containing 85 mg/L MS222 through the mouth, which also maintained the anesthetic condition of the fish. Then, we injected BDA iontophoretically following the protocol reported elsewhere (Yamamoto and Ito, 2008), with a shorter injection time (5 min) adjusting for the small brain size of zebrafish. After the injection, the cranial opening was closed with a small piece of Saran Wrap that was affixed to the cranium with an acrylic adhesive (Aron alpha, jelly type; Toagosei). Postoperative fish were maintained in aquaria for 1-3 hours. After the survival period, the fish were deeply anesthetized with MS222 (over 300 mg/L) and perfused through the heart with 4% paraformaldehyde in 0.1 M phosphate buffer, pH7.4 (PB). The brains were removed from the skull and post-fixed in fresh solution of the same fixative at 4ºC for 3 hours. Tissue processing and double labeling for BDA and Pvalb7 were performed as described previously (Yamamoto et al., 1998). Briefly, the fixed brains were embedded in 5% agarose (Sigma, type IX, ultra-low gelling temperature) containing 20% sucrose and frozen in n-hexane at -60ºC. Then, transverse sections were cut at a thickness of 30 µm on a cryostat. Sections were then incubated with anti-Pvalb7 antibody (1:1,000) in 0.05 M Tris-HCl-buffered saline, 0.1% Tween (TBST) containing 1% normal goat serum (Sigma, G9023) overnight at room temperature. After washes, the sections were incubated for 4 hours with TBST solution containing CF™ 568 goat anti-mouse IgG [H+L] antibody (1:100, 20301, Biotium) and streptavidin-CF 488A (1: 50, 29034, Biotium). The sections were coverslipped with 0.1 M PB containing 20%

sucrose after washing. The fluorescence images were obtained with the LSM700 confocal laser-scanning microscope.

2.7. Bodian staining

Bodian staining is a highly reproducible silver impregnation protocol that has been used to visualize nerve fibers in the mouse brain (Blume et al., 2017). Zebrafish brain was embedded in paraffin and sectioned at 7-μm thickness. After deparaffinization and rehydration, the sections were incubated in 70% ethanol overnight, incubated in 1% potassium dichromate solution for 1 h at room temperature, and washed with distilled water (DW) three times. The sections were then incubated in 1% silver protein (Merck) for 24 h at 37 $_{o}$C with copper pieces, in a glass staining pot. The staining pot was removed from the incubator and cooled to room temperature, and the sections were washed with DW. The sections were then incubated in 1% chloroauric acid for 1 h, washed with DW, incubated in 2% oxalic acid for 5 min, washed with DW, incubated in 5% sodium thiosulfate for 5 min, and washed with DW. The silver-stained sections were dehydrated by ethanol and xylene, and mounted with EUKITT mounting medium (O. Kindler & ORSAtec) and covered with a cover glass. The sections were photographed using a NanoZoomer slide scanner (Hamamatsu Photonics).

2.8. Bielschowsky staining

Bielschowsky staining was performed using a previously described protocol (Litchfield and Nagy, 2001) that was modified as described below. Brains were cryoprotected with

30% sucrose in PBS, and sectioned at 20-μm thickness using a freezing microtome (REM-700, Yamato Kohki Industrial Co., Ltd.). The brain sections were mounted on slide glass and dried overnight at room temperature. After rehydration with DW, the sections were placed in 10% silver nitrate (solution I) at 37 ^{o}C for 30 min in the dark, then washed with DW three times. Ammonium hydroxide was added to the 10% silver nitrate until the precipitate disappeared (solution II), and the washed sections were placed in this solution at 37 ^{o}C for 15 min in the dark. The sections were then washed with 0.3% ammonium hydroxide three times for 2 min each. The stock solution for color development was 20% formalin, 0.5% citric acid (trisodium dehydrate), and 0.05% nitric acid. The developing solution was prepared by adding the stock solution to solution II to become 0.2% and gently mixed, immediately before use. The sections were placed in the developing solution at room temperature. The stained sections were monitored under a microscope. When satisfactory staining was obtained, the reaction was stopped by washing with DW and then treating the sections with 5% sodium thiosulfate for 5 min. The stained sections were dehydrated with ethanol and xylene and mounted with EUKITT medium and covered with a cover glass.

2.9. Laser ablation

Laser ablation of the GC axons was performed using an LSM780-DUO-NLO laser-scanning inverted microscope (Zeiss) equipped with a Ti-sapphire femtosecond pulse laser (Chameleon Vision II, Coherent) as described previously (Hamamura et al., 2014; Takeuchi et al., 2015b).

2.10. Statistics

Data were analyzed for statistical significance and graphs were generated using Microsoft Excel and Graphpad PRISM (ver 5.1).

3. Results

3.1. Reln, Vldlr, and Dab1a are required for proper PC migration in zebrafish

Zebrafish have only one gene for *reln*. *reln* is expressed in GCs in the cerebellum, as in mammals (Costagli et al., 2002; Takeuchi et al., 2017) (Suppl. Fig. S2). To examine the roles of Reln signaling in neural development, we generated a *reln* mutant by CRISPR/Cas9 that has a deletion in the genomic region encoding the second Reln repeat, which introduces a premature stop codon (*reln*$^{\Delta 7}$, Suppl. Fig. S1). We also analyzed *reln*$^{\Delta 28}$ and *vldlr*$^{+13}$, which were reported previously (Di Donato et al., 2018), and *dab1a*$^{\Delta 14}$, which was generated by a CRISPR/Cas9 method as described previously, but contains a deletion that is different from the published mutant allele (Di Donato et al., 2018) (Suppl. Fig. S1). Both *reln*$^{\Delta 7}$ and *reln*$^{\Delta 28}$ homozygotes showed a severe decrease in *reln* transcripts at an early larval stage (5 days post fertilization, dpf) (Suppl. Fig. S2), probably due to nonsense-mediated RNA decay. These observations indicated that these *reln* mutations were probably null alleles.

The *reln*$^{\Delta 7}$, *reln*$^{\Delta 28}$, *vldlr*$^{+13}$, and *dab1a*$^{\Delta 14}$ mutants showed no abnormalities in PC development or in the layer formation at 5 dpf (Suppl. Fig. S3). Adult fish of these mutants showed no hypoplasia of the cerebellum, which was the same size as in wild-type (Fig. 2). However, the adult cerebellum of these mutants showed abnormal PC positioning. In wild-type fish, the parvalbumin7 (Pvalb7)-expressing PCs were located in the PCL, and ectopic PCs were rare (Fig. 2A, B). In contrast, the number of PCs was reduced in the PCL, and more PCs were detected in the internal GCLs in the *reln*$^{\Delta 7}$, *reln*$^{\Delta 28}$, *vldlr*$^{+13}$, and *dab1a*$^{\Delta 14}$ mutants, to similar extents (Fig. 2C-K, Suppl. Fig. S4). The proportion of PCs that was ectopic (located in the GCL) was significantly higher in these mutants compared to wild-type (Fig. 2L). The *reln*$^{\Delta 7}$ mutants showed no abnormalities in the Neurod1^{+} GC development (Suppl. Fig. S5), indicating that the GCs were not affected in the *reln* mutants. These findings together revealed that Reln-VLDLR-Dab1 signaling is required for the proper migration of the PCs but not for the differentiation of PCs and GCs in zebrafish after the initial neurogenesis of the cerebellum. Although VLDLR and ApoER2 function redundantly in the mouse cerebellum (Trommsdorff et al., 1999), and zebrafish has two *dab1* genes, *dab1a* and *dab1b* (Costagli et al., 2006; Herrero-Turrion et al., 2010; Imai et al., 2012), our data suggest that Vldlr and Dab1a have at least partly non-redundant roles in the Reln-mediated PC migration.

3.2. Ectopic PCs aberrantly receive afferent fibers in the reln and dab1a mutants

It has not been clear whether mouse mutants deficient in Reln signaling display abnormal cerebellar neural circuits, because severe cerebellar hypoplasia hinders the investigation of neural circuits in these mutants. PCs receive two afferent axons: GC axons (called parallel fibers, PF) and climbing fibers (CFs), which originate from neurons in the inferior olivary nuclei (IO neurons). We used Vglut1 (Slc17a7a) as a marker for GC axons in the cerebellum (Bae et al., 2009). We found aberrant axonal projections of Vglut1^{+} GC axons to dendrite regions of the ectopic PCs (located in the GCL) in the *reln*$^{\Delta 7}$, *reln*$^{\Delta 28}$, *vldlr*$^{+13}$, and *dab1a*$^{\Delta 14}$ mutants (Fig. 2). The CFs can be immunostained with an anti-calretinin antibody (Bae et al., 2009) or marked using the IO neuron-specific Gal4 line hspGFFDMC28C (28C) and the reporter line UAS:GFP (Takeuchi et al., 2015a). In the wild-type cerebellum, the calretinin-immunoreactive (CR-ir) signals were detected in the PCL or the deep region of the ML, where the proximal dendrites of PCs receive the CFs (Bae et al., 2009) (Fig. 3A-D). In the *reln*$^{\Delta 7}$ or *dab1a*$^{\Delta 14}$ adult cerebellum, CR-ir signals were also detected in the vicinity of the ectopic PC somata (Fig. 3E-L). Similarly, the 28C; UAS:GFP signals were detected in the PCL and in the deep ML in the wild-type cerebellum, whereas they were also detected near the ectopic PC somata in the mutants. In addition, some 28C; UAS:GFP^{+} CF axons were colocalized with Pvalb7^{+} PC dendrites in the mutants (Fig. 3R-T). Although the structure of the IOs but not the CF projection is affected in *reeler* mutant mice (Blatt and Eisenman, 1988; Goffinet, 1979; Katsuyama and Terashima, 2009), the IO neurons marked by 28C; UAS:GFP developed normally in the zebrafish *reln*$^{\Delta 7}$ mutants (Suppl. Fig. S6). These data together indicate that the ectopic PCs and/or PC

dendrites receive aberrant afferent axons of PFs and CFs from normal GCs and IO neurons, respectively, in Reln-signaling-deficient mutants.

3.3. Migration of ECs and BGs is also disturbed in reln mutants

ECs are projection neurons in the cerebellum of ray-finned fish that receive axons of PCs and GCs, and send efferent axons outside the cerebellum (Butler and Hodos, 2005; Ikenaga et al., 2006). ECs are identified as cells whose soma is surrounded by Pvalb7^{+} PC axons but does not express Pvalb7 itself (Bae et al., 2009). A portion of the ECs can be marked using the Gal4 trap line hspGFFgDMC156A and UAS:GFP (Takeuchi et al., 2015a) (Fig. 4). We examined both hspGFFgDMC156A; UAS:GFP-positive and -negative ECs (GFP^{+} ECs and GFP^{-} ECs, respectively). Both types of ECs were located in the vicinity of the PCL in wild-type adult cerebellum (Fig. 4A-D), while some ECs were also ectopically located in the GCL of the *reln*$^{\Delta 7}$ mutant adult cerebellum (Fig. 4E-H). The proportion of ectopic ECs (GCL/Total, for both types) was significantly higher in the *reln*$^{\Delta 7}$ mutants than in wild-type (Fig. 4I-N), indicating that Reln is involved in the proper positioning of ECs.

BGs can be marked using the Gal4 trap line SA(LF)251A (Takeuchi et al., 2015a). The cell bodies of BGs were located in the vicinity of PCs, and the BGs extended glial processes into the ML in the control SA(LF)251A; UAS:GFP adult cerebellum (Bae et al., 2009; Takeuchi et al., 2015a) (Fig. 5A-D), while *reln*$^{\Delta 7}$ mutant SA(LF)251A; UAS:GFP cerebellum additionally showed ectopic GFP signals in the region of the GCL where ectopic PCs were also detected (Fig. 5E-H). The proportion of

the ectopic BG area (including the cell body and the processes) was higher in *reln*$^{\Delta 7}$ mutants compared to wild-type (Fig. 5I). These data indicate that Reln is involved in positioning both ECs and BGs in addition to PCs in zebrafish.

3.4. Reln signaling is required for type I neuron migration in the cerebellum-like structure in the mesencephalic tectum

The gross morphology and layer structure of the mesencephalic tectum were not significantly affected in the *reln*$^{\Delta 7}$ mutants (Suppl. Fig. S4 and S7). However, we found abnormalities in the cerebellum-like structure in the mesencephalic tectum of these mutants. The cerebellum-like structure in the mesencephalic tectum contains two major components: type I neurons and granule cells. Pvalb7 and Vglut1 are markers for the somata and dendrites of type I neurons and for the axons of GCs in the TL, respectively, in the optic tectum (Bae et al., 2009) (Suppl. Fig. S8, S9, S10). The Pvalb7^{+} somata of type I neurons were located in the stratum fibrosum et griseum superficiale (SFGS) layer and extended their dendrites to the superficial layer called the stratum marginale (SM), where they received the Vglut1^{+} axons of GCs, in the wild-type adult cerebellum (Fig. 6A-F, Suppl. Fig. S9), as previously described for other teleost fish (Meek and Schellart, 1978; Xue et al., 2003). However, in the *reln*$^{\Delta 7}$, *reln*$^{\Delta 28}$, *vldlr*$^{+13}$, and *dab1a*$^{\Delta 14}$ mutants, only a small population of type I neurons remained in the SFGS; ectopic type I neurons were seen in deeper (ventral) regions and aberrantly extended their dendrites in the optic tectum (Fig. 6G-X, Suppl. Fig. S9, data not shown for *reln*$^{\Delta 28}$). Further examination of the position of type I neurons in the optic tectum revealed that

significantly more type I neurons were present in the deeper regions in *reln*$^{\Delta 7}$, *vldlr*$^{+13}$, and *dab1a*$^{\Delta 14}$ mutants, compared to wild-type fish (Fig. 6Y). These type I neurons were not located more superficially than those in wild-type fish. Ectopic type I neurons were also confirmed by the expression of transcripts for Grid2 interacting protein a (grid2ipa), a principal cell marker, in ectopic positions (Takeuchi et al., 2017) (Suppl. Fig. S11). These data collectively indicate that Reln signaling is required for the proper positioning of type I neurons. Furthermore, although the GC axons were present in the SM, they projected aberrantly to deeper regions near the ectopic type I neurons. The aberrant GC axons often co-localized with dendrites of the ectopic type I neurons (Fig. 6G-X). These data also suggest that, as the dendrites of the ectopic PCs received the GC axons in the cerebellum, the dendrites of ectopic type I neurons received the GC axons in the cerebellum-like structure in the mesencephalic tectum.

3.5. Reln signaling controls PC migration through the regulation of PC polarity

PCs are continuously generated during the larval stages (one month) in zebrafish (Kani et al., 2010; Kaslin et al., 2013). We next examined the PCs in *reln*$^{\Delta 7}$ mutants at the middle larval (15 dpf) and early juvenile stage (30 dpf, Fig. 7). In wild-type larvae at 15 dpf, Pvalb7^{+} migrating PCs that had not reached the PCL were observed in the GCL, where they radially extended a leading process toward the ML (Fig. 7A-C). In *reln*$^{\Delta 7}$ mutants, migrating PCs in the GCL were also observed. However, many of these PCs extended one or multiple neurites in aberrant directions (Fig. 7D-H). At 30 dpf, more PCs were still in the GCL in the *reln*$^{\Delta 7}$ mutants compared to wild-type fish (Fig. 7J).

These data suggest that Reln signaling controls the cell polarity of migrating PCs, and that the abnormal cell polarity may be related to the slow migration of PCs in the *reln* mutants.

3.6. Reln protein is localized to the superficial layer of the cerebellum and the cerebellum-like structure

In early-stage larvae and juvenile fish, *reln* transcripts are detected in the GCs in the TL of the mesencephalic tectum and in the GCs in the cerebellar GCL (Costagli et al., 2002) (Suppl. Fig. S8). Reln protein is localized to the superficial layer of the tectum in early-stage larvae (Di Donato et al., 2018). We further examined the localization of Reln protein in the cerebellum and the tectum at the early juvenile stage (30 dpf) and in adults (Fig. 8). Immunostaining with an anti-Reln antibody showed that Reln protein was highly localized to the SM, where the Vglut1^{+} GC axons were present, and relatively weakly localized to a deeper layer of the tectum (i.e., the stratum opticum, SO). Strong staining for Reln was also observed in the ML of the cerebellum and the crista cerebellaris (CC) in the rostro-dorsal hindbrain, where GC axons were present. Reln was also weakly detected in the TL and the GCL, where the somata of GCs were located (Fig. 8A-H, Q, R). These Reln signals were not detected in *reln*$^{\Delta 7}$ mutants. These data indicate that, although *reln* transcripts are expressed by differentiated GCs in the TL and the GCL, Reln protein is mainly localized to the superficial layers of the tectum and the cerebellum. Thus, there should be a mechanism by which Reln is

transferred from the GC somata in the TL and the GCL to the superficial layers in the tectum and the cerebellum.

3.7. Reln localization is dependent on GC axons

Reln protein was detected in the cerebellum and the CC from 4-dpf, when the GCs started to differentiate (Suppl. Fig. S13, S14). We found that Reln signals colocalized or overlapped with GC axons, which were visualized by the GC-specific Gal4 line hspGFFDMC90A or by Vglut1, in the cerebellum and the CC at 5 dpf (Suppl. Fig. S14, S15, S16). To obtain deeper insight into the relationship between Reln and the GC axons, we carried out two experiments: laser ablation of the GC axons (Suppl. Fig. S14) and loss of an axonal transport component (Suppl. Fig. S15, S16). In the first experiment, we applied a laser to the left side to specifically ablate GC axon bundles in the CC, which project to crest cells in the dorsal hindbrain, at 4 dpf (Suppl. Fig. S14). As a result, the Reln was strongly reduced in the left CC at 5 dpf. The ratio of Reln protein in the right versus left CC was significantly higher in the treated larvae compared to the control non-treated larvae. In the second experiment, we inhibited the axonal transport in GCs using mutants for kinesin I, which functions as a motor protein complex in axon transport. Our previous RNA-seq analysis revealed that *kif5aa* and *kif5ba* encode major components of kinesin I in the GCs in zebrafish (Takeuchi et al., 2017). Although *kif5aa* or *kif5ba* single mutants showed no apparent abnormality in the GC axons or Reln localization (Suppl. Fig. S15), *kif5aa*; *kif5ba* double mutants showed GC bundles (marked by Vglut1) that were reduced in length and thickness, and less

Reln protein in the caudal region of the CC (Suppl. Fig. S16). These data collectively suggest that the GC axons is required for proper localization of Reln protein.

Discussion

4.1 Role of Reln signaling in cerebellum development in zebrafish

The PC migration defect in zebrafish *reln* mutants (Fig. 2) was less severe than that seen in mouse *reeler* mutants (Heckroth et al., 1989; Katsuyama and Terashima, 2009; Mariani et al., 1977; Yuasa et al., 1993). This was not due to the presence of a *reln* ortholog (*reelin, like* is seen in the database ZFIN: https//zfin.org, but it is part of the *reln* gene). Rather, it was at least partly due to the lack of GC reduction in the zebrafish *reln* mutants (Suppl. Fig. S5) (discussed below). It is also possible that the role of Reln in PC migration is slightly different between mouse and zebrafish. In mouse, early/posterior-born PCs migrate tangentially from the VZ and change their orientation to form the PC plate, and this process strongly depends on Reln (Miyata et al., 2010). Although a precise analysis of the PC migration in zebrafish is required, the tangential migration and orientation change might be specific for mammalian PCs. At the mid-larval zebrafish stage, migrating PCs were observed in the GCL in both wild-type and *reln* mutants (Fig. 7), and these PCs were derived from the entire area (not specifically the posterior region) of the VZ. These radially migrating PCs extended one or multiple neurites in a random manner in *reln* mutants (Fig. 7), suggesting that Reln controls the migration of PCs by regulating cell polarity or the generation of neurites.

This process is similar to the migration of cortical neurons in the mammalian neocortex, in which a small amount of Reln is present in the intermediated zone (IZ) and the subventricular zone (SVZ) (Uchida et al., 2009; Yoshida et al., 2006), where it controls the transition of neurons from a multipolar to bipolar morphology (Britto et al., 2011; Hack et al., 2007; Jossin and Cooper, 2011; Uchida et al., 2009). In zebrafish, a small amount of Reln was detected in the TL and the GCL (Fig. 8). Reln may also control the change in the cell polarity of PCs in the zebrafish cerebellum in a manner similar to the mouse neocortex, in which Reln signaling is reported to control the positioning of the Golgi apparatus and thereby to regulate the formation of the leading process (primary dendrite) in cortical neurons and PCs (Dillon et al., 2017; Matsuki et al., 2010; Miyata et al., 2010). We previously reported that the Golgi apparatus is located at the root of the primary dendrites in PCs in early-stage zebrafish larvae (Tanabe et al., 2010). Thus, Reln-mediated control of the Golgi localization may regulate the cell polarity and thereby the radial migration of PCs in zebrafish.

Mouse *reeler* mutants, *Vldlr/ApoER2* double mutants, and *Dab1* mutants show cerebellar hypoplasia (Howell et al., 1997; Katsuyama and Terashima, 2009; Mariani et al., 1977; Mikoshiba et al., 1980; Sheldon et al., 1997; Sweet et al., 1996; Trommsdorff et al., 1999; Yoneshima et al., 1997), whereas the zebrafish *reln*, *vldlr*, and *dab1a* mutants did not (Fig. 2). In amniote cerebella, Sonic hedgehog (Shh) is secreted from PCs and positively controls the proliferation of GC progenitors in the EGL (Dahmane and Ruiz i Altaba, 1999; Lewis et al., 2004; Wallace, 1999; Wechsler-Reya and Scott, 1999). The migration defect of the PCs in Reln signaling-deficient mice

probably separates the GC progenitors from PCs, resulting in a reduction in the Shh-dependent proliferation of GCs. In zebrafish, although *shh* is reported to be expressed in the ECs but not PCs (Biechl et al., 2016), *ptc1*, a downstream target of Shh signaling, is not expressed in the larval cerebellum (Chaplin et al., 2010), suggesting that Shh signaling is not involved in the proliferation of GC progenitors in this species (Hibi et al., 2017). Therefore, the migration defect in PCs did not lead to a reduction in GCs or to cerebellar hypoplasia in the zebrafish *reln*, *vldlr*, and *dab1a* mutants.

We found that the radial migration of BGs and ECs was abnormal in the zebrafish *reln* mutants (Fig. 4, 5). The abnormal positioning of BGs is also seen in mouse *reeler* mutants (Terashima et al., 1985). BGs are thought to be derived from the VZ in the mammalian cerebellum (Yuasa, 1996). In the zebrafish cerebellum, most of the *olig2*-expressing ECs are derived from the VZ (Kani et al., 2010). Therefore, it is likely that both BGs and ECs radially migrate from the VZ to the vicinity of the PCL in the zebrafish cerebellum. Our findings collectively suggest that Reln signaling controls the radial migration of BGs and ECs that are born in the VZ, as it does for PCs.

Although we observed ectopic PCs, BGs, and ECs in the *reln* mutant cerebellum, they were not located more superficially than those in the wild-type cerebellum, and many of these cells were positioned normally (Fig. 2, 4, 5). Therefore, Reln is not the only factor controlling the migration of these cells; other factor(s) must be involved in stopping their migration in the right place.

4.2 Role of Reln signaling in development of the cerebellum-like structure in zebrafish

We found that most of the type I neurons were ectopically localized in deep regions of the tectum in the zebrafish Reln and Reln-signaling mutants (Fig. 6). This phenotype was similar to the abnormal localization of layer-V cortical neurons in mouse *reeler* mutants, in which the layer-V neurons are scattered across the neocortex (Boyle et al., 2011; Dekimoto et al., 2010; Hertel and Redies, 2011), suggesting that Reln signaling has a similar role in the migration of type I neurons in zebrafish and cortical neurons in mice. It is completely unknown where the zebrafish type I neurons are born and how they migrate to reach to the SFGS. The developmental process of GCs in the TL of zebrafish is also not known. Given that the migration of type I neurons is regulated in the same manner as that of PCs, it is tempting to speculate that type I neurons are generated in the VZ of the tectum and migrate radially, and that Reln controls the radial migration of type I neurons in the tectum as it does for PCs in the cerebellum. We found strong and relatively weak localizations of Reln in the SM and the SO, respectively (Fig. 8). Reln is reported to form a concentration gradient in the tectum in early-stage larvae (Di Donato et al., 2018). The concentration gradient of Reln in the tectum may be involved in the attraction of type I neurons. Alternatively, Reln may function as a permissive factor to promote the radial migration of type I neurons.

Reln-deficient mouse and rat mutants show abnormal layer formation in the optic tectum (Baba et al., 2007; Sakakibara et al., 2003). There are no cerebellum-like structures in the mammalian tectum, and it is not clear which cells are mispositioned in the tectum of these mammalian mutants. One possibility is that Reln signaling is involved in the migration of multiple cell types in the tectum in both mammals and

zebrafish. However, the general layer structure of the tectum was not affected in the zebrafish *reln* mutants (Suppl. Fig. S4, S7). Although further analysis is required to clarify this issue, our data indicate that Reln signaling is at least required for the proper migration of type I neurons in the tectum in zebrafish. Our findings indicate that the cerebellum and the cerebellum-like structure exploit a similar Reln-dependent mechanism for the migration of their principal cells.

Reln is reported to function as a chemoattractant for the axons of retinal ganglion cells (RGCs) in zebrafish (Di Donato et al., 2018). As type I neurons also receive RGC axons in goldfish (Meek, 1981), the abnormal positioning of type I neurons (and possibly other neurons) may affect the retinal projection. Taking previous findings together with our present results, Reln signaling controls the projection of RGC axons directly by activating VLDR/Dab1 in the RGC axons, and also indirectly by regulating the position of target cells, which controls afferent projections.

4.3 *Axonal transport of Reln*

In zebrafish, the *reln* mRNA is strongly localized to the GCL, but not the ML (Costagli et al., 2002) (Suppl. Fig. S8). In mouse, the *Reln* mRNA is strongly localized to the EGL in the cerebellum primordium (D'Arcangelo et al., 1995). Nevertheless, in both mouse and zebrafish, Reln protein was detected in the superficial domain of the cerebellum (Fig. 8) (Miyata et al., 1996; Miyata et al., 2010; Schiffmann et al., 1997). Similarly, the *reln* mRNA in zebrafish is expressed in the TL where mature GCs are located (Costagli et al., 2002) (Suppl. Fig. S8), while Reln protein was detected in the

superficial domains of the tectum (Fig. 8). Reln protein was also weakly detected in the GCL and the TL. These data together suggest that Reln is translated in the somata of mature GCs in the GCL and TL, and then Reln is transported from the somata to the superficial layer of the cerebellum and cerebellum-like structures. The colocalization of Reln and GC axons in the tectum, the cerebellum, and the CC (Fig. 8, Suppl. Fig. S14) suggest that Reln is transported in the GC axons. The localization of Reln to the axons of GCs and Cajal-Retzius cells was also reported previously (Derer et al., 2001; Miyata et al., 1996). We found that laser ablation of the GC axons perturbed the localization of Reln in the CC (Suppl. Fig. S14), suggesting that GC axons are required for the distribution of Reln at least in the dorsal hindbrain. Furthermore, *kif5aa*; *kif5ba*-double mutants showed decreased Reln localization to the caudal CC, which was correlated with shortened GC axons (Suppl. Fig. S15, S16). Kinesin I may function to transport Reln as well as other components necessary for axonal elongation. Although we cannot exclude the possibility that Reln is secreted from the somata of GCs (or other types of cells), diffuses, and sticks to the GC axons in the CC, our data together with the localization of Reln in GC axons in mouse suggest that axonal transport in GCs is a major mechanism for the localization of Reln protein to the CC, and most likely to the cerebellum and the tectum as well. It was previously reported that Reln expression by the *Nestin* promoter rescues the PCL formation defect in *reeler* mutants (Magdaleno et al., 2002). The axonal transport-dependent redistribution of Reln might contribute to this rescue. We found that Reln was distributed in a wider region than the GC axon-rich layer SM in the tectum (Fig. 8), suggesting that Reln is distributed from the GC axons,

and this distribution probably depends on the extracellular environment of the neural tissue.

4.4 Model for Reln-mediated cell positioning in the cerebellum and the cerebellum-like structure

In mouse, *VLDLR* and *Dab1* are expressed in PCs during development (Miyata et al., 2010). Although we did not detect the specific expression of *vldr* and *dab1a* in PCs, ECs, BGs or type I neurons by in situ hybridization, due to their low expression levels in zebrafish larvae, our previous RNA-seq analysis revealed that *vldlr* and *dab1a* are expressed in the PCs at the mid-larval stage (Takeuchi et al., 2017). These data suggest that Reln directly activates VLDLR-Dab1-mediated signaling in PCs and possibly in ECs, BGs, and type I neurons, as well. In the *reln*, *vldlr*, and *dab1a* mutants, ectopic PCs and type I neurons received afferent GC axons, and ectopic PCs also received CF axons (Fig. 2, 3, and 6). Thus, it is unlikely that Reln directly controls the axon guidance of PFs and CFs by activating signaling in the GCs and the IO neurons. The ectopic PCs and type I neurons may attract these afferent fibers independently of Reln signaling.

Considering all the data, we propose a model for the Reln-mediated regulation of cell migration in the cerebellum and the cerebellum-like structure in zebrafish (Fig. 9). In the cerebellum, GCs are born in the rhombic lip (at the early larval stage) or later in the ML. The GCs extend their axons and ventrally migrate to the GCL (GCs in the EG and the LCa do not migrate ventrally). The differentiated GCs in the GCL express

reln transcripts that are translated in the soma. The Reln protein is transported from the soma to the ML through GC axons, and this transport is probably mediated by kinesin-related motor proteins. Reln functions as a chemoattractant that promotes the radial migration of PCs, ECs, and BGs from the VZ (it may also function to stop them at the boundary between the ML and the GCL). The PCs then attract the afferent fibers, PFs and CFs, possibly by expressing some guidance molecules. In the tectum, the processes by which the GCs and type I neurons start migrating are unknown. However, although further studies are required, a similar or the same mechanism is likely to be involved in the migration of type I neurons and the formation of the cerebellum-like neural circuits. Our findings shed light on the mechanism that controls neural circuit formation of the cerebellum and the cerebellum-like structures. Zebrafish Reln signaling mutants provide a good model system for analyzing the roles of Reln-mediated neural development and understanding Reln-related human diseases (Guidotti et al., 2016; Ishii et al., 2016; Lammert and Howell, 2016; Yu et al., 2016).

Acknowledgments

We thank K. Kawakami and the National Bioresource Project for providing the zebrafish transgenic lines, M. Kinoshita and F. Zhang for the hSpCas9 plasmids, Y. Tsukazaki and K. Kondoh for fish mating and care, T. Higashiyama for use of the laser-scanning microscope, and the members of the Hibi Laboratory for helpful

discussions. This work was supported by JSPS KAKENHI Grant Numbers JP15H04376, JP18H02448 (to M.H.) and JP18K06333 to (T. S.).

References

Ansai, S., Kinoshita, M., 2014. Targeted mutagenesis using CRISPR/Cas system in medaka. Biology open 3, 362-371.

Auer, T.O., Xiao, T., Bercier, V., Gebhardt, C., Duroure, K., Concordet, J.P., Wyart, C., Suster, M., Kawakami, K., Wittbrodt, J., Baier, H., Del Bene, F., 2015. Deletion of a kinesin I motor unmasks a mechanism of homeostatic branching control by neurotrophin-3. eLife 4.

Baba, K., Sakakibara, S., Setsu, T., Terashima, T., 2007. The superficial layers of the superior colliculus are cytoarchitectually and myeloarchitectually disorganized in the reelin-deficient mouse, reeler. Brain research 1140, 205-215.

Bae, Y.K., Kani, S., Shimizu, T., Tanabe, K., Nojima, H., Kimura, Y., Higashijima, S., Hibi, M., 2009. Anatomy of zebrafish cerebellum and screen for mutations affecting its development. Developmental biology 330, 406-426.

Bell, C.C., 2002. Evolution of cerebellum-like structures. Brain Behav Evol 59, 312-326.

Bell, C.C., Han, V., Sawtell, N.B., 2008. Cerebellum-like structures and their implications for cerebellar function. Annu Rev Neurosci 31, 1-24.

Biechl, D., Dorigo, A., Koster, R.W., Grothe, B., Wullimann, M.F., 2016. Eppur Si Muove: Evidence for an External Granular Layer and Possibly Transit Amplification in the Teleostean Cerebellum. Front Neuroanat 10, 49.

Blatt, G.J., Eisenman, L.M., 1988. Topographic and zonal organization of the olivocerebellar projection in the reeler mutant mouse. The Journal of comparative neurology 267, 603-615.

Blume, M., Inoguchi, F., Sugiyama, T., Owada, Y., Osumi, N., Aimi, Y., Taki, K., Katsuyama, Y., 2017. Dab1 contributes differently to the morphogenesis of the hippocampal subdivisions. Development, growth & differentiation 59, 657-673.

Boyle, M.P., Bernard, A., Thompson, C.L., Ng, L., Boe, A., Mortrud, M., Hawrylycz, M.J., Jones, A.R., Hevner, R.F., Lein, E.S., 2011. Cell-type-specific consequences of Reelin deficiency in the mouse neocortex, hippocampus, and amygdala. The Journal of comparative neurology 519, 2061-2089.

Britto, J.M., Tait, K.J., Johnston, L.A., Hammond, V.E., Kalloniatis, M., Tan, S.S., 2011. Altered speeds and trajectories of neurons migrating in the ventricular and subventricular zones of the reeler neocortex. Cerebral cortex 21, 1018-1027.

Butler, A.B., Hodos, H., 2005. Comparative Vertebrate Neuroanatomy: Evolution and Adaptation, Second Edition. Wiley-Liss, New York.

Campbell, P.D., Heim, A.E., Smith, M.Z., Marlow, F.L., 2015. Kinesin-1 interacts with Bucky ball to form germ cells and is required to pattern the zebrafish body axis. Development 142, 2996-3008.

Caviness, V.S., Jr., 1973. Time of neuron origin in the hippocampus and dentate gyrus of normal and reeler mutant mice: an autoradiographic analysis. The Journal of comparative neurology 151, 113-120.

Chaplin, N., Tendeng, C., Wingate, R.J., 2010. Absence of an external germinal layer in zebrafish and shark reveals a distinct, anamniote ground plan of cerebellum development. The Journal of neuroscience : the official journal of the Society for Neuroscience 30, 3048-3057.

Cong, L., Ran, F.A., Cox, D., Lin, S., Barretto, R., Habib, N., Hsu, P.D., Wu, X., Jiang, W., Marraffini, L.A., Zhang, F., 2013. Multiplex genome engineering using CRISPR/Cas systems. Science 339, 819-823.

Costagli, A., Felice, B., Guffanti, A., Wilson, S.W., Mione, M., 2006. Identification of alternatively spliced dab1 isoforms in zebrafish. Dev Genes Evol 216, 291-299.

Costagli, A., Kapsimali, M., Wilson, S.W., Mione, M., 2002. Conserved and divergent patterns of Reelin expression in the zebrafish central nervous system. The Journal of comparative neurology 450, 73-93.

D'Arcangelo, G., Homayouni, R., Keshvara, L., Rice, D.S., Sheldon, M., Curran, T., 1999. Reelin is a ligand for lipoprotein receptors. Neuron 24, 471-479.

D'Arcangelo, G., Miao, G.G., Chen, S.C., Soares, H.D., Morgan, J.I., Curran, T., 1995. A protein related to extracellular matrix proteins deleted in the mouse mutant reeler. Nature 374, 719-723.

Dahmane, N., Ruiz i Altaba, A., 1999. Sonic hedgehog regulates the growth and

patterning of the cerebellum. Development 126, 3089-3100.
Dekimoto, H., Terashima, T., Katsuyama, Y., 2010. Dispersion of the neurons expressing layer specific markers in the reeler brain. Development, growth & differentiation 52, 181-193.
Derer, P., Derer, M., Goffinet, A., 2001. Axonal secretion of Reelin by Cajal-Retzius cells: evidence from comparison of normal and Reln(Orl) mutant mice. The Journal of comparative neurology 440, 136-143.
Di Donato, V., De Santis, F., Albadri, S., Auer, T.O., Duroure, K., Charpentier, M., Concordet, J.P., Gebhardt, C., Del Bene, F., 2018. An Attractive Reelin Gradient Establishes Synaptic Lamination in the Vertebrate Visual System. Neuron 97, 1049-1062 e1046.
Dillon, G.M., Tyler, W.A., Omuro, K.C., Kambouris, J., Tyminski, C., Henry, S., Haydar, T.F., Beffert, U., Ho, A., 2017. CLASP2 Links Reelin to the Cytoskeleton during Neocortical Development. Neuron 93, 1344-1358 e1345.
Falconer, D.S., 1951. Two new mutants, 'trembler' and 'reeler', with neurological actions in the house mouse (Mus musculus L.). J Genet 50, 192-201.
Folgueira, M., Sueiro, C., Rodriguez-Moldes, I., Yanez, J., Anadon, R., 2007. Organization of the torus longitudinalis in the rainbow trout (Oncorhynchus mykiss): an immunohistochemical study of the GABAergic system and a DiI tract-tracing study. The Journal of comparative neurology 503, 348-370.
Goffinet, A.M., 1979. An early development defect in the cerebral cortex of the reeler mouse. A morphological study leading to a hypothesis concerning the action of the mutant gene. Anatomy and embryology 157, 205-216.
Guidotti, A., Grayson, D.R., Caruncho, H.J., 2016. Epigenetic RELN Dysfunction in Schizophrenia and Related Neuropsychiatric Disorders. Frontiers in cellular neuroscience 10, 89.
Hack, I., Hellwig, S., Junghans, D., Brunne, B., Bock, H.H., Zhao, S., Frotscher, M., 2007. Divergent roles of ApoER2 and Vldlr in the migration of cortical neurons. Development 134, 3883-3891.
Hamamura, Y., Nishimaki, M., Takeuchi, H., Geitmann, A., Kurihara, D., Higashiyama, T., 2014. Live imaging of calcium spikes during double fertilization in Arabidopsis. Nat Commun 5, 4722.
Hashimoto, M., Hibi, M., 2012. Development and evolution of cerebellar neural circuits.

Development, growth & differentiation 54, 373-389.
Hatten, M.E., Heintz, N., 1995. Mechanisms of neural patterning and specification in the developing cerebellum. Annu Rev Neurosci 18, 385-408.
Heckroth, J.A., Goldowitz, D., Eisenman, L.M., 1989. Purkinje cell reduction in the reeler mutant mouse: a quantitative immunohistochemical study. The Journal of comparative neurology 279, 546-555.
Herrero-Turrion, M.J., Velasco, A., Arevalo, R., Aijon, J., Lara, J.M., 2010. Characterisation and differential expression during development of a duplicate Disabled-1 (Dab1) gene from zebrafish. Comparative biochemistry and physiology. Part B, Biochemistry & molecular biology 155, 217-229.
Hertel, N., Redies, C., 2011. Absence of layer-specific cadherin expression profiles in the neocortex of the reeler mutant mouse. Cerebral cortex 21, 1105-1117.
Hibi, M., Matsuda, K., Takeuchi, M., Shimizu, T., Murakami, Y., 2017. Evolutionary mechanisms that generate morphology and neural-circuit diversity of the cerebellum. Development, growth & differentiation 59, 228-243.
Hibi, M., Shimizu, T., 2012. Development of the cerebellum and cerebellar neural circuits. Dev Neurobiol 72, 282-301.
Hiesberger, T., Trommsdorff, M., Howell, B.W., Goffinet, A., Mumby, M.C., Cooper, J.A., Herz, J., 1999. Direct binding of Reelin to VLDL receptor and ApoE receptor 2 induces tyrosine phosphorylation of disabled-1 and modulates tau phosphorylation. Neuron 24, 481-489.
Hirota, Y., Nakajima, K., 2017. Control of Neuronal Migration and Aggregation by Reelin Signaling in the Developing Cerebral Cortex. Frontiers in cell and developmental biology 5, 40.
Howell, B.W., Hawkes, R., Soriano, P., Cooper, J.A., 1997. Neuronal position in the developing brain is regulated by mouse disabled-1. Nature 389, 733-737.
Howell, B.W., Herrick, T.M., Cooper, J.A., 1999. Reelin-induced tyrosine [corrected] phosphorylation of disabled 1 during neuronal positioning. Genes Dev 13, 643-648.
Howell, B.W., Herrick, T.M., Hildebrand, J.D., Zhang, Y., Cooper, J.A., 2000. Dab1 tyrosine phosphorylation sites relay positional signals during mouse brain development. Current biology : CB 10, 877-885.
Hwang, W.Y., Fu, Y., Reyon, D., Maeder, M.L., Tsai, S.Q., Sander, J.D., Peterson, R.T., Yeh, J.R., Joung, J.K., 2013. Efficient genome editing in zebrafish using a CRISPR-Cas

system. Nature biotechnology 31, 227-229.
Ikenaga, T., Yoshida, M., Uematsu, K., 2006. Cerebellar efferent neurons in teleost fish. Cerebellum 5, 268-274.
Imai, H., Oomiya, Y., Kikkawa, S., Shoji, W., Hibi, M., Terashima, T., Katsuyama, Y., 2012. Dynamic changes in the gene expression of zebrafish Reelin receptors during embryogenesis and hatching period. Development, growth & differentiation 54, 253-263.
Ishii, K., Kubo, K.I., Nakajima, K., 2016. Reelin and Neuropsychiatric Disorders. Frontiers in cellular neuroscience 10, 229.
Ito, H., Yamamoto, N., Yoshimoto, M., Sawai, N., Yang, C.Y., Xue, H.G., Imura, K., 2003. Fiber connections of the torus longitudinalis in a teleost: Cyprinus carpio re-examined. The Journal of comparative neurology 457, 202-211.
Jao, L.E., Wente, S.R., Chen, W., 2013. Efficient multiplex biallelic zebrafish genome editing using a CRISPR nuclease system. Proc Natl Acad Sci U S A 110, 13904-13909.
Jossin, Y., Cooper, J.A., 2011. Reelin, Rap1 and N-cadherin orient the migration of multipolar neurons in the developing neocortex. Nat Neurosci 14, 697-703.
Kani, S., Bae, Y.K., Shimizu, T., Tanabe, K., Satou, C., Parsons, M.J., Scott, E., Higashijima, S., Hibi, M., 2010. Proneural gene-linked neurogenesis in zebrafish cerebellum. Developmental biology 343, 1-17.
Kaslin, J., Kroehne, V., Benato, F., Argenton, F., Brand, M., 2013. Development and specification of cerebellar stem and progenitor cells in zebrafish: from embryo to adult. Neural development 8, 9.
Katsuyama, Y., Oomiya, Y., Dekimoto, H., Motooka, E., Takano, A., Kikkawa, S., Hibi, M., Terashima, T., 2007. Expression of zebrafish ROR alpha gene in cerebellar-like structures. Dev Dyn 236, 2694-2701.
Katsuyama, Y., Terashima, T., 2009. Developmental anatomy of reeler mutant mouse. Development, growth & differentiation 51, 271-286.
Kojima, T., Nakajima, K., Mikoshiba, K., 2000. The disabled 1 gene is disrupted by a replacement with L1 fragment in yotari mice. Brain Res Mol Brain Res 75, 121-127.
Kuo, G., Arnaud, L., Kronstad-O'Brien, P., Cooper, J.A., 2005. Absence of Fyn and Src causes a reeler-like phenotype. The Journal of neuroscience : the official journal of the Society for Neuroscience 25, 8578-8586.
Lammert, D.B., Howell, B.W., 2016. RELN Mutations in Autism Spectrum Disorder.

Frontiers in cellular neuroscience 10, 84.
Lee, G.H., D'Arcangelo, G., 2016. New Insights into Reelin-Mediated Signaling Pathways. Frontiers in cellular neuroscience 10, 122.
Lewis, P.M., Gritli-Linde, A., Smeyne, R., Kottmann, A., McMahon, A.P., 2004. Sonic hedgehog signaling is required for expansion of granule neuron precursors and patterning of the mouse cerebellum. Developmental biology 270, 393-410.
Litchfield, S., Nagy, Z., 2001. New temperature modification makes the Bielschowsky silver stain reproducible. Acta Neuropathol 101, 17-21.
Magdaleno, S., Keshvara, L., Curran, T., 2002. Rescue of ataxia and preplate splitting by ectopic expression of Reelin in reeler mice. Neuron 33, 573-586.
Mali, P., Yang, L., Esvelt, K.M., Aach, J., Guell, M., DiCarlo, J.E., Norville, J.E., Church, G.M., 2013. RNA-guided human genome engineering via Cas9. Science 339, 823-826.
Mariani, J., Crepel, F., Mikoshiba, K., Changeux, J.P., Sotelo, C., 1977. Anatomical, physiological and biochemical studies of the cerebellum from Reeler mutant mouse. Philos Trans R Soc Lond B Biol Sci 281, 1-28.
Matsuki, T., Matthews, R.T., Cooper, J.A., van der Brug, M.P., Cookson, M.R., Hardy, J.A., Olson, E.C., Howell, B.W., 2010. Reelin and stk25 have opposing roles in neuronal polarization and dendritic Golgi deployment. Cell 143, 826-836.
Meek, J., 1981. A Golgi-electron microscopic study of goldfish optic tectum. I. Description of afferents, cell types, and synapses. The Journal of comparative neurology 199, 149-173.
Meek, J., Schellart, N.A., 1978. A Golgi study of goldfish optic tectum. The Journal of comparative neurology 182, 89-122.
Mikami, Y., Yoshida, T., Matsuda, N., Mishina, M., 2004. Expression of zebrafish glutamate receptor delta2 in neurons with cerebellum-like wiring. Biochem Biophys Res Commun 322, 168-176.
Mikoshiba, K., Nagaike, K., Kohsaka, S., Takamatsu, K., Aoki, E., Tsukada, Y., 1980. Developmental studies on the cerebellum from reeler mutant mouse in vivo and in vitro. Developmental biology 79, 64-80.
Miyata, T., Nakajima, K., Aruga, J., Takahashi, S., Ikenaka, K., Mikoshiba, K., Ogawa, M., 1996. Distribution of a reeler gene-related antigen in the developing cerebellum: an immunohistochemical study with an allogeneic antibody CR-50 on normal and reeler

mice. The Journal of comparative neurology 372, 215-228.
Miyata, T., Nakajima, K., Mikoshiba, K., Ogawa, M., 1997. Regulation of Purkinje cell alignment by reelin as revealed with CR-50 antibody. The Journal of neuroscience : the official journal of the Society for Neuroscience 17, 3599-3609.
Miyata, T., Ono, Y., Okamoto, M., Masaoka, M., Sakakibara, A., Kawaguchi, A., Hashimoto, M., Ogawa, M., 2010. Migration, early axonogenesis, and Reelin-dependent layer-forming behavior of early/posterior-born Purkinje cells in the developing mouse lateral cerebellum. Neural development 5, 23.
Northmore, D.P., 2017. Holding visual attention for 400millionyears: A model of tectum and torus longitudinalis in teleost fishes. Vision Res 131, 44-56.
Ogawa, M., Miyata, T., Nakajima, K., Yagyu, K., Seike, M., Ikenaka, K., Yamamoto, H., Mikoshiba, K., 1995. The reeler gene-associated antigen on Cajal-Retzius neurons is a crucial molecule for laminar organization of cortical neurons. Neuron 14, 899-912.
Ota, S., Hisano, Y., Muraki, M., Hoshijima, K., Dahlem, T.J., Grunwald, D.J., Okada, Y., Kawahara, A., 2013. Efficient identification of TALEN-mediated genome modifications using heteroduplex mobility assays. Genes to cells : devoted to molecular & cellular mechanisms 18, 450-458.
Sakakibara, S., Misaki, K., Terashima, T., 2003. Cytoarchitecture and fiber pattern of the superior colliculus are disrupted in the Shaking Rat Kawasaki. Brain Res Dev Brain Res 141, 1-13.
Sawtell, N.B., Bell, C.C., 2008. Adaptive processing in electrosensory systems: links to cerebellar plasticity and learning. J Physiol Paris 102, 223-232.
Schiffmann, S.N., Bernier, B., Goffinet, A.M., 1997. Reelin mRNA expression during mouse brain development. The European journal of neuroscience 9, 1055-1071.
Sekine, K., Kubo, K., Nakajima, K., 2014. How does Reelin control neuronal migration and layer formation in the developing mammalian neocortex? Neurosci Res 86, 50-58.
Sheldon, M., Rice, D.S., D'Arcangelo, G., Yoneshima, H., Nakajima, K., Mikoshiba, K., Howell, B.W., Cooper, J.A., Goldowitz, D., Curran, T., 1997. Scrambler and yotari disrupt the disabled gene and produce a reeler-like phenotype in mice. Nature 389, 730-733.
Sweet, H.O., Bronson, R.T., Johnson, K.R., Cook, S.A., Davisson, M.T., 1996. Scrambler, a new neurological mutation of the mouse with abnormalities of neuronal migration. Mamm Genome 7, 798-802.

Takeuchi, M., Matsuda, K., Yamaguchi, S., Asakawa, K., Miyasaka, N., Lal, P., Yoshihara, Y., Koga, A., Kawakami, K., Shimizu, T., Hibi, M., 2015a. Establishment of Gal4 transgenic zebrafish lines for analysis of development of cerebellar neural circuitry. Developmental biology 397, 1-17.

Takeuchi, M., Yamaguchi, S., Sakakibara, Y., Hayashi, T., Matsuda, K., Hara, Y., Tanegashima, C., Shimizu, T., Kuraku, S., Hibi, M., 2017. Gene expression profiling of granule cells and Purkinje cells in the zebrafish cerebellum. The Journal of comparative neurology 525, 1558-1585.

Takeuchi, M., Yamaguchi, S., Yonemura, S., Kakiguchi, K., Sato, Y., Higashiyama, T., Shimizu, T., Hibi, M., 2015b. Type IV Collagen Controls the Axogenesis of Cerebellar Granule Cells by Regulating Basement Membrane Integrity in Zebrafish. PLoS genetics 11, e1005587.

Tanabe, K., Kani, S., Shimizu, T., Bae, Y.K., Abe, T., Hibi, M., 2010. Atypical protein kinase C regulates primary dendrite specification of cerebellar Purkinje cells by localizing Golgi apparatus. The Journal of neuroscience : the official journal of the Society for Neuroscience 30, 16983-16992.

Terashima, T., Inoue, K., Inoue, Y., Mikoshiba, K., Tsukada, Y., 1985. Observations on Golgi epithelial cells and granule cells in the cerebellum of the reeler mutant mouse. Brain research 350, 103-112.

Trommsdorff, M., Gotthardt, M., Hiesberger, T., Shelton, J., Stockinger, W., Nimpf, J., Hammer, R.E., Richardson, J.A., Herz, J., 1999. Reeler/Disabled-like disruption of neuronal migration in knockout mice lacking the VLDL receptor and ApoE receptor 2. Cell 97, 689-701.

Uchida, T., Baba, A., Perez-Martinez, F.J., Hibi, T., Miyata, T., Luque, J.M., Nakajima, K., Hattori, M., 2009. Downregulation of functional Reelin receptors in projection neurons implies that primary Reelin action occurs at early/premigratory stages. The Journal of neuroscience : the official journal of the Society for Neuroscience 29, 10653-10662.

Wallace, V.A., 1999. Purkinje-cell-derived Sonic hedgehog regulates granule neuron precursor cell proliferation in the developing mouse cerebellum. Current biology : CB 9, 445-448.

Ware, M.L., Fox, J.W., Gonzalez, J.L., Davis, N.M., Lambert de Rouvroit, C., Russo, C.J., Chua, S.C., Jr., Goffinet, A.M., Walsh, C.A., 1997. Aberrant splicing of a mouse

disabled homolog, mdab1, in the scrambler mouse. Neuron 19, 239-249.
Wechsler-Reya, R.J., Scott, M.P., 1999. Control of neuronal precursor proliferation in the cerebellum by Sonic Hedgehog. Neuron 22, 103-114.
Westerfield, M., 2000. The zebrafish book: a guide for the laboratory use of zebrafish.
Wullimann, M.F., 1994. The teleostean torus longitudinalis: a short review on its structure, histochemistry, connectivity, possible function and phylogeny. Eur J Morphol 32, 235-242.
Wullimann, M.F., Mueller, T., Distel, M., Babaryka, A., Grothe, B., Koster, R.W., 2011. The long adventurous journey of rhombic lip cells in jawed vertebrates: a comparative developmental analysis. Front Neuroanat 5, 27.
Xue, H.G., Yamamoto, N., Yang, C.Y., Kerem, G., Yoshimoto, M., Imura, K., Ito, H., 2003. Fiber connections of the torus longitudinalis and optic tectum in holocentrid teleosts. The Journal of comparative neurology 462, 194-212.
Yamamoto, N., Ito, H., 2008. Visual, lateral line, and auditory ascending pathways to the dorsal telencephalic area through the rostrolateral region of the lateral preglomerular nucleus in cyprinids. The Journal of comparative neurology 508, 615-647.
Yamamoto, N., Oka, Y., Yoshimoto, M., Sawai, N., Albert, J.S., Ito, H., 1998. Gonadotropin-releasing hormone neurons in the gourami midbrain: a double labeling study by immunocytochemistry and tracer injection. Neurosci Lett 240, 50-52.
Yoneshima, H., Nagata, E., Matsumoto, M., Yamada, M., Nakajima, K., Miyata, T., Ogawa, M., Mikoshiba, K., 1997. A novel neurological mutant mouse, yotari, which exhibits reeler-like phenotype but expresses CR-50 antigen/reelin. Neurosci Res 29, 217-223.
Yoshida, M., Assimacopoulos, S., Jones, K.R., Grove, E.A., 2006. Massive loss of Cajal-Retzius cells does not disrupt neocortical layer order. Development 133, 537-545.
Yu, N.N., Tan, M.S., Yu, J.T., Xie, A.M., Tan, L., 2016. The Role of Reelin Signaling in Alzheimer's Disease. Molecular neurobiology 53, 5692-5700.
Yuasa, S., 1996. Bergmann glial development in the mouse cerebellum as revealed by tenascin expression. Anatomy and embryology 194, 223-234.
Yuasa, S., Kawamura, K., Ono, K., Yamakuni, T., Takahashi, Y., 1991. Development and migration of Purkinje cells in the mouse cerebellar primordium. Anatomy and embryology 184, 195-212.
Yuasa, S., Kitoh, J., Oda, S., Kawamura, K., 1993. Obstructed migration of Purkinje

cells in the developing cerebellum of the reeler mutant mouse. Anatomy and embryology 188, 317-329.

FIGURE LEGENDS

Fig. 1. Structure of cerebellum and mesencephalic tectum

Schematic presentation of zebrafish cerebellum, mesencephalic tectum, and neural circuits in these structures. (A) Sagittal section image of cerebellum and mesencephalic tectum. Neural circuits (transverse section images) in the cerebellum (B) and the cerebellum-like structure (C). BG, Bergmann glial cell; Cb, cerebellum; CF, climbing fiber; EC, eurydendroid cell; GC, granule cell; GCL, granule cell layer; IO, inferior olivary nucleus; LCa, lobes caudalis cerebelli; MF, mossy fiber; ML, molecular layer; PC, Purkinje cell; PCL, Purkinje cell layer; PrCN: precerebellar nucleus; SAC, stratum album centrale; SC, stellate cell; SFGS, stratum fibrosum et griseum superficiale; SGC, stratum griseum centrale; SM, stratum marginale; SO, stratum opticum; SPV, stratum periventriculare; TeO, tectum opticum; TL, torus longitudinalis.

Fig. 2. Aberrant positioning of Purkinje cells (PCs) in adult zebrafish *reln*, *vldlr*, and *dab1a* mutants

(A-J) Sagittal sections of the brain from adult (90-150 dpf) wild-type (WT, A-A”, *n*=6), and *reln* (C-C”, E-E”, *n*=5 for $reln^{\Delta7/\Delta7}$ and *n*=5 for $reln^{\Delta28/\Delta28}$), $vldlr^{+13/+13}$ (G-G”, *n*=5), and $dab1a^{\Delta14/\Delta14}$ (I-I”, *n*=8) mutant zebrafish were stained with anti-parvalbumin7 (Pvalb7, magenta) and anti-Vglut1 (green) antibodies. Typical cerebellum images are shown. (B-B”, D-D”, F-F”, H-H”, J-J”) High magnification images of the boxes in A”, C,” E”, G, and I”. Ectopic Purkinje cells (PCs) are indicated by arrowheads. Axonal projections of granule cells (GCs) to ectopic PCs are marked by dotted circles. (K)

Ectopic PCs. Sagittal sections 14-μm thick were prepared from adult zebrafish WT (*n*=7), and *reln*$^{Δ7/Δ7}$ (*n*=8), *vldlr*$^{+13/+13}$ (*n*=5), and *dab1a*$^{Δ14/Δ14}$ (*n*=12) mutant brains. Pvalb7^{+} PCs in the granule cell layer (GCL) or the Purkinje cell layer (PCL) were counted in every fourth section (14 total sections near the midline of each fish). Average numbers and standard deviations of PCs in the GCL, PCL, or all layers (Total) are shown in the graph. (L) Proportion of PCs in the GCL in WT, and *reln*$^{Δ7/Δ7}$, *vldlr*$^{+13/+13}$, and *dab1a*$^{Δ14/Δ14}$ mutant cerebellum. A greater proportion of the total PCs were located in the GCL in the *reln*, *vldlr*, and *dab1a* mutants than in WT. * $p < 0.05$; ** $p < 0.01$; *** $p < 0.001$; ns not significant (Dunnett's test for K and Dunn's multiple comparison test for L). Scale bars: 100 μm in A (applies to A-A", C-C", E-E", G-G", I-I"); 50 μm in B, D, F, H, and J (applies to B-B", D-D", F-F", H-H" and J-J", respectively).

Fig. 3. Projection of climbing fibers (CFs) to ectopic PCs in *reln* and *dab1a* mutants

(A-L) Calretinin-immunoreactive (CR-ir^{+}) axonal projections to PCs. Sagittal sections of adult (92-dpf) WT (A-D, *n*=4) and *reln*$^{Δ7/Δ7}$ mutant (E-L, *n*=4) brains were stained with anti-Pvalb7 (magenta) and anti-calretinin antibodies (green). (B-D, F-H, J-L) High magnification images of the boxes in A, E, and I. Typical images are shown. CR-ir^{+} axons projected to ectopic PCs located in the GCL in *reln* mutant cerebella, but not in WT cerebella. (M-T) CF projections to ectopic PCs. Sagittal section of adult (96 dpf) hspGFFDMC28C (28C); UAS:GFP fish brains, which express GFP in the CFs (axons of the neurons in the inferior olivary nuclei), harboring WT (control, *n*=4) or homozygous *reln* mutant (*reln*$^{Δ7/Δ7}$, *n*=4) alleles were stained with anti-Pvalb7 (magenta), and

anti-GFP (green) antibodies. GFP+ CFs projected to ectopic PCs located in the GCL in *reln* mutant cerebella, but not in WT cerebella. Ectopic somata and dendrites of PCs are indicated by asterisks and arrowheads. CR-ir+ and 28C; UAS:GFP+ axons projecting to the ectopic Purkinje cells are indicated by arrows. The abbreviations are described in the legend for Fig. 1. Scale bars: 200 μm in A (applies to A, E, and I); 20 μm in B (applies to B-D, F-H, J-L); 200 μm in M (applies to M and Q); 20 μm in N (applies to R-T).

Fig. 4. Ectopic eurydendroid cells (ECs) in *reln* mutants

(A-H) Ectopic ECs in *reln*$^{\Delta 7/\Delta 7}$ mutants. Sagittal sections of adult (96-dpf) hspGFFgDMC156A; UAS:GFP zebrafish brains, which express GFP in ECs, harboring WT (control, *n*=6) or homozygous *reln* mutant (*reln*$^{\Delta 7/\Delta 7}$, *n*=7) alleles were stained with anti-Pvalb7 (magenta), anti-GFP (green) antibodies, and Hoechst (nucleus, cyan). (B-D, F-H) High magnification images of the boxes in A and E. There are two types of ECs: GFP+ (indicated by arrowheads) and GFP- (asterisks) ECs, both of which receive the Pvalb7+ axons of PCs (somata are surrounded by Pvalb7+ axons). Ectopic GFP+ and GFP- ECs were observed in the GCL of the *reln* mutant cerebellum (E-H). (I-K) GFP+ (I), GFP- (J), and total (J) ECs in the GCL, the PCL, or all layers (Total) of the controls and *reln*$^{\Delta 7/\Delta 7}$ mutants were counted in every fourth section (18 total sections near the midline in each fish). Average numbers and standard deviations of ECs in the GCL, PCL, or all layers (Total) are shown in graphs. (L-N) Proportion of GFP+ (L), GFP- (M), or total (N) ECs in the GCL in controls and *reln*$^{\Delta 7/\Delta 7}$ mutants. * $p < 0.05$; ** $p < 0.01$; ns

not significant (Student's *t* test for J; Welch's *t* test for I and K; Mann-Whitney test for L-N). Scale bars: 200 μm in A (applies to A and E); 40 μm in B (applies to B-D, F-H).

Fig. 5. Ectopic Bergmann glial cells (BGs) in *reln* mutants

(A-H) Aberrant localization of BGs in *reln* mutants. Sagittal section of adult (96 dpf) SAGFF(LF)251A; UAS:GFP brains, which express GFP in BGs, harboring WT (control, *n*=5) or homozygous *reln* mutant (*reln*$^{Δ7/Δ7}$, *n*=5) alleles were stained with anti-Pvalb7 (magenta) and anti-GFP (green) antibodies. (B-D, F-H) High magnification images of the boxes in A and E. (I) Ratio of the BG (GFP^{+}) area in the GCL to the total BG area in controls and *reln*$^{Δ7/Δ7}$ mutants. Fluorescence images were captured of every fourth section (16 total sections in each fish). The GFP^{+} area in the Pvalb7-negative GCL layer was measured and divided by the total GFP^{+} area in the cerebellum. * p <0.05 (Mann-Whitney U test). Scale bars: 300 μm in A (applies to E); 50 μm in B (applies to B-D and F-H).

Fig. 6. Aberrant positioning of type I neurons in adult zebrafish *reln, vldlr,* and *dab1a* mutants

(A-X) Cross sections of the brain from adult (90-150 dpf) WT (A-F, *n*=9) and *reln*$^{Δ7/Δ7}$ (G-L, *n*=5), *vldlr*$^{+13/+13}$ (M-R, *n*=5), and *dab1a*$^{Δ14/Δ14}$ (S-X, *n*=4) mutant zebrafish were stained with anti- Pvalb7 (magenta) and anti-Vglut1 (green). Typical tectum images are shown. (D-F, J-L, P-R, V-X) High magnification images of the boxes in C, I, O, and U. Typical images are shown. Pvalb7^{+} type I neurons were located in a restricted area of

the stratum fibrosum et griseum superficiale (SFGS) layer in the tectum in WT (A, D), but were ectopically localized in *reln*, *vldlr*, and *dab1a* mutants (indicated by asterisks in G, J, M, P, S, and V). Dendrites of some type I neurons were misoriented (indicated by arrowheads in J, P, and V). The Vglut1+ axons of granule cells (GCs) in the tectum project to dendrites of type I neurons in the stratum marginale (SM) in WT (B, E). These axons projected to ectopic type I neurons in *reln*, *vldlr*, and *dab1a* mutants (indicated by arrows in H, K, N, Q, T, and W). The stratum opticum (SO) is located between the SM and the SFGS. (Y) Position of type I neurons in WT (*n*=9), *reln*$^{\Delta 7/\Delta 7}$ (*n*=4), *vldlr*$^{+13/+13}$ (*n*=4), and *dab1a*$^{\Delta 14/\Delta 14}$ (*n*=4). The tectum region was divided into ten domains from the pia to ventricle. The positions of the type I neurons were determined by measuring the distance between the pia and the soma of type I neurons. Pvalb7+ cells located in the vicinity of the ventricular zone that had a morphology different from type I neurons were excluded. Average and standard deviation are indicated in the graph. * $p < 0.05$; ** $p < 0.01$; *** $p < 0.001$; ns not significant (Dunn's multiple comparison test). Scale bars: 20 μm in A (applies to A-C, G-I, M-O, and S-U); 40 μm in D (applies to D-F, J-L, P-R, and V-X).

Fig. 7. Defects in the migration and polarity of PCs in *reln* mutants.

Sagittal sections of the brain from WT (A-C, *n*=4) and *reln*$^{\Delta 7/\Delta 7}$ (D-H, *n*=4) 15-dpf larvae, and from WT (I, *n*=3) and *reln*$^{\Delta 7/\Delta 7}$ (J, *n*=3) 30-dpf fish, were stained with anti-Pvalb7 (magenta) and anti-Vglut1 (green) antibodies, and Hoechst (cyan). Typical cerebellum images are shown. The ventral limit of the cerebellum is indicated by a

dotted line. (Ba, Ca, Da, Ea, Fa, Ga, and Ha) High magnification images of the PCs marked by “a” in B-H. The Pvalb7 and Vglut1-double positive region marks the ML. Migrating PCs were detected in the GCL in WT, and they extended a neurite (primary dendrite) toward the pial side (Ba, Ca, *n*=4). Many of the migrating cells extended one or multiple neurites in aberrant directions in the *reln*$^{\Delta 7/\Delta 7}$ mutants (Ea, Fa, Ga, Ha, *n*=4). At 30 dpf, most of the PCs had reached the PCL in WT (I), whereas many ectopic PCs were detected in the GCL in *reln*$^{\Delta 7/\Delta 7}$ mutants (J, *n*=3). The abbreviations are described in the legend for Fig. 1. Scale bars: 20 μm in A (applies to A-H); 100 μm in I (applies to J).

Fig. 8. Localization of Reln protein in the tectum and the cerebellum.

Medial and lateral sagittal sections of the brain from 30-dpf (A-P) and 90-dpf (Q-T) WT and *reln*$^{\Delta 7/\Delta 7}$ mutant zebrafish were stained with anti-Reln (magenta), anti-Vglut1 (green), and Hoechst (cyan). Three fish for 30-dpf and one fish for 90-dpf WT or *reln*$^{\Delta 7/\Delta 7}$ mutant fish were analyzed. Typical images are shown. (E-H, M-P) High magnification images of the boxes in C, D, K, and L. In WT, Reln protein was detected strongly in the SM and relatively weakly in the SO in the TeO. Reln was also detected strongly in the ML in the Cb. Weak Reln signals were also detected in the GCs in the TL and the GCL. These signals were absent in *reln*$^{\Delta 7/\Delta 7}$ mutants. CC, crista cerebellaris. The other abbreviations are described in the legend for Fig. 1. Scale bars: 100 μm in A (applies to A-D, I-L); 50 μm in E (applies to E-H, M-P); 200 μm in Q (applies to Q-T).

Fig. 9. Schematic diagram of the role of Reln signaling in the layer and neural circuit formation of the cerebellum and the mesecephalic tectum in zebrafish.

reln mRNA (*reelin*) and Reln protein (Reelin) are indicated by black and green letters, respectively. The somata of principal cells (PCs and type I neurons), BGs, and ECs are indicated by purple, orange, and yellow circles, respectively. Please see Discussion for details. The abbreviations are described in the legend for Fig. 1.

Supplementary Data

Fig. S1. Zebrafish *reln*, *vldlr*, and *dab1a* mutants.

Structure of wild-type and mutant Reln (A), Vldlr (B), and Dab1a (C). Reln has eight unique repeats (reelin repeats), each centered around an epidermal growth factor (EGF)-like cysteine pattern. A bar indicates the binding domain for the receptors (A). Vldlr has low-density lipoprotein receptor class A domains (LDLa), a coagulation factor Xa inhibitory site (FXa), calcium-binding EGF-like domains (EGF-CA), low-density lipoprotein-receptor YWTD domains (LY), and a low-density lipoprotein receptor repeat class B domain (Ldl_re) (B). Dab1a has a P-loop NTPase domain (Pl) and a phosphotyrosine-binding domain (PTB) (C). The nature of the mutations is also indicated. $reln^{\Delta 7}$ was established in this work. $reln^{\Delta 28}$, $vldlr^{+13}$, $vldlr^{\Delta 9}$, and $dab1a^{\Delta 14}$ were established previously (Di Donato et al., 2018). Red arrows indicate the positions corresponding to indel mutations. Red letters indicate inserted nucleotides. Amino acid numbers (aa) of the prospective wild-type and mutant proteins are indicated.

Fig. S2. *reln* transcripts are severely decreased in *reln* mutants.

Expression of *reln* in 5-dpf WT (A, D, *n*=2), *reln*$^{\Delta 7/\Delta 7}$ (B, E, *n*=2), and *reln*$^{\Delta 28/\Delta 28}$ (C, F, *n*=2) larvae was analyzed by whole-mount in situ hybridization. Note that the *reln* expression was severely decreased in the *reln* mutants. Cb, cerebellum. Scale bars: 100 μm in A.

Fig. S3. Cerebellum development is not affected in *reln* or *dab1a* mutant early-stage larvae.

WT (A-D, *n*=8), *reln*$^{\Delta 7/\Delta 7}$ (E-H, *n*=5), *reln*$^{\Delta 28/\Delta 28}$ (I-L, *n*=9), and *dab1a*$^{\Delta 14/\Delta 14}$ (M-P, *n*=11) larvae at 5 dpf were stained with anti-Pvalb7 (magenta) and anti-Vglut1 (green) antibodies. Dorsal views with anterior to the left (A-C, E-G, I-K, M-O). Sagittal section images at the level indicated by lines in C, G, K, and O are shown in D, H, L, and P. Typical images are shown. Note that no abnormalities in the development of Pvalb7^{+} PCs or Vglut1^{+} GC axons or in the layer formation were observed in the *reln* and *dab1b* mutants. CC, crest cerebellaris. The other abbreviations are described in the legend of Fig. 1. Scale bars: 100 μm in A (applies to A-C, E-G, I-K, M-O); 20 μm in D (applies to D, H, L, P).

Fig. S4. Morphology of the cerebellum and the mesencephalic tectum in *reln* mutants.

Cross sections of the cerebellum (A-D) and the mesencephalon (E-H) of adult WT (A, E,

G, *n*=2) and *reln*$^{\Delta 7/\Delta 7}$ mutant (B, C, D, F, and H, *n*=2) fish were stained by the Bodian silver impregnation method, which visualizes neuronal fibers (gray) and cell nuclei (purple). (C, D) High magnification images of the *reln*$^{\Delta 7/\Delta 7}$ mutant cerebellum. Arrows indicate ectopic neurons that have a large soma and are probably PCs in the GCL. (G, H) High magnification images of the WT and *reln*$^{\Delta 7/\Delta 7}$ mutant tectum. Note that no gross abnormalities in the tectum of the *reln* mutant were observed. Scale bars: 100 μm in A (applies to A, B); C (applies to C, D); E (applies to E, F); and G (applies to G, H).

Fig. S5. Granule cell (GC) development is not affected in *reln* mutants.

Sagittal sections of the brain from adult (93-dpf) WT (A, B) and *reln*$^{\Delta 7/\Delta 7}$ (C, D) fish were stained with anti-Neurod1 antibodies, which mark the nucleus of immature and mature GCs in the TL, ML, and GCL. Note that the number and position of GC somata were largely unaffected in the *reln* mutants (*n*=6 for WT, and *n*=6 for *reln*$^{\Delta 7/\Delta 7}$ mutants). The abbreviations are described in the legend of Fig. 1. Sale bars: 100 μm in A (applies to A, C); 200 μm in B (applies to B, D).

Fig. S6. Inferior olivary nuclei (IOs) are not affected in *reln* mutants.

Sagittal section of the brain from adult (90-150-dpf) control (A, B, *n*=4) and *reln*$^{\Delta 7/\Delta 7}$ mutant (C, D, *n*=4) fish with hspGFFDM28C; UAS:GFP, which marks the neurons in the IOs and their axons (CFs). (B, D) High magnification images of the boxes in A and C. Typical images are shown. Note that the number and position of the IO neurons were unaffected in the *reln* mutants. The abbreviations are described in the legend of Fig. 1.

Scale bars: 40 μm in A (applies to A, C); 100 μm in B (applies to B, D).

Fig. S7. Layer structure of the optic tecum is not affected in *reln* mutants.

Cross sections of the mesencephalon of adult WT (A, C, *n*=2) and *reln*$^{\Delta 7/\Delta 7}$ mutant (B, D, *n*=2) fish were stained by the Bielschowsky silver impregnation method, which visualizes neuronal fibers. (C, D) High magnification images of the tectum. Note that there was no difference in the neuronal fiber structure between the WT and the *reln* mutant tectum. Scale bars: 100 μm in A (applies to A, B) and C (applies to C, D).

Fig. S8. Expression of *pvalb7*, *vglut1*, and *reln* in the mesencephalic tectum and the cerebellum.

Cross sections of the mesencephalon (A-D, G-I) and the cerebellum (E, F, J, K) of adult WT zebrafish were stained with antisense riboprobes of *pvalb7* (A, B), *vglut1* (C-F), or *reln* (G-K) genes. (B, D, F, H, I, K) High magnification images of the boxes in A, C, E, G, H, and J. Note that *pvalb7*-expressing cells are located in the SFGS of the tectum (A, B), and *reln* and *vglut1* are not detected in the superficial layer of the tectum and the cerebellum (D, F, H, I). The abbreviations are described in the legend of Fig. 1. Scale bars: 200 μm in A, C, E, G, J; 100 μm in B, D, F, H, I, K.

Fig. S9. Pvalb7 is a marker for type I neuron.

(A-C) Tracing of type I neurons. Biotinylated dextran amine (BDA) was injected into the SM of the tectum. After incubation, transverse sections were labeled with

immunofluorescence using anti-Pvalb7 antibody (magenta) and fluorescent streptavidin (green). Note that the neurons labeled with BDA are also positive for Pvalb7 (indicated by arrows). (D-G) High magnification, grayscale images of Pvalb7-positive cells in Fig. 6D, J, P, and V. Scale bars: 50 μm in A (applies to A-C) and D (applies to D-G).

Fig. S10. Granule cells in the TL send their axons to the SM in the tectum.

Cross sections of a tectum region of the brain from adult hspGFFDMC90A;UAS:GFP fish, which express GFP specifically in GCs in the TL and the cerebellum, were stained with anti-GFP (green) and anti-Neurod1 (magenta) antibodies, and Hoechst (cyan). (B, C, D, F, G, H) High magnification images of the boxes in A, C, E, and G. Note that GFP was detected in the SM, the TL, and the GCL. The abbreviations are described in the legend of Fig. 1. Scale bars: 200 μm in A and E, 100 μm in C, D (applies to D', D"), and G, 50 μm in B (applies to B, B', B"); F (applies to F, F', F"); and H (applies to H, H', H").

Fig. S11. Ectopic type I neurons and Purkinje cells (PCs) in *reln* mutants.

Sagittal sections from the brain of adult (159-dpf) WT (A-C, *n*=2) and *reln*$^{\Delta 7/\Delta 7}$ (D-F, *n*=2) zebrafish were stained with an antisense riboprobe for Grid2 interacting protein a (grid2ipa). *grid2ipa* transcripts were detected in type I neurons located in the SFGS of the TeO, and in PCs in the PCL of the Cb in WT. Ectopic *grid2ipa*-expressing type I neurons and PCs were observed in the *reln*$^{\Delta 7/\Delta 7}$ mutants (indicated by arrows). The abbreviations are described in the legend of Fig. 1. Scale bars: 100 μm in A (applies to

A, D); 50 μm in B (applies to B, E); 50 μm in C (applies to C, F).

Fig. S12. Reln is not colocalized with dendrites of PCs in the ML of the cerebellum.

Sagittal sections of the brain from adult *Tg(aldoca:gap43-Venus)* fish, which express Venus in PCs, were stained with anti-GFP (Venus) and anti-Reln (magenta) antibodies, and Hoechst (cyan). Confocal optical sections (0.93 μm thickness). (B-D) High magnification images of the box in A. Note that Reln is not colocalized with PC dendrites. Scale bars: 200 μm in A; 10 μm in C (applies to B-D).

Fig. S13. Specific detection of Reln protein by immunostaining

WT (A, *n*=4) and *reln*$^{\Delta 7/\Delta 7}$ (B, *n*=3) larvae at 5-dpf were stained with anti-Reln (magenta) antibody. Dorsal views with anterior to the left. Typical images are shown. Note that Reln signals in and near the granule cell axons were severely decreased in the *reln* mutants. In some *reln* mutant larvae, nonspecific signals were also seen bilaterally in the hindbrain (marked by arrowheads). Scale bars: 100 μm in A.

Fig. S14. Axon-dependent localization of Reln protein in GCs.

(A-I) GC axons and Reln localization. hspGFFDMC90A; UAS:GFP larvae, which express GFP in the soma and axons of GCs, were stained at 3-dpf (A-C), 4-dpf (D-F), and 5-dpf (G-I) with anti-GFP (green) and anti-Reln (magenta) antibodies. Typical data are shown. Reln was detected in or near GC axons in the cerebellum (Cb) and the crista cerebellaris (CC). (J, K) Ablation of GC axons. GC axons in the CC of 4-dpf

hspGFFDMC90A; UAS:GFP larvae were ablated by a laser on the left side. (Ja, b) High magnification views of the left GC axons before (Ja) and after the ablation (Ja'). The point of the laser ablation is indicated by red lines. After the ablation, the larvae were reared and subjected to immunostaining with anti-GFP and anti-Reln antibodies at 5 dpf (K). Dorsal views with anterior to the left. Scale bars: 50 μm in A (applies to A-I, K-M); 50 μm in J; 20 μm (applies to Ja, Jb). (N) Fluorescence intensity of Reln signals on the right and left side (ROI, region of interest) in control (H, *n*=23) and laser-treated larvae (L, *n*=29) was measured. The ratio of the signal on the right to left side in each larva was calculated and plotted in a graph. The ratio was significantly different in the laser-treated larvae (*** $p<0.001$; Mann-Whitney test).

Fig. S15. Reln and GC axons in kinesin mutants.

WT (A-D, *n*=4), *kif5aa*$^{*162/*162}$ (E-H, *n*=13), *kif5ba*$^{ae12/ae12}$ (I-L, *n*=4), and *kif5aa*$^{*162/*162}$*; kif5ba*$^{ae12/ae12}$ (M-P, *n*=7) larvae at 5-dpf were stained with anti-Reln (magenta) and anti-Vglut1 (green) antibodies. Dorsal views with anterior to the left. (B-D, F-H, J-L, N-P) High magnification images of the boxes in A, E, I, and M. Typical images are shown. Note that the Reln and Vglut1 stainings were not strongly affected in the *kif5aa*$^{*162/*162}$ and *kif5ba*$^{ae12/ae12}$ single mutants, whereas they were decreased in the double mutants (indicated by arrows in N). Detailed analysis of the double mutants is shown in Fig. S1. Scale bars: 200 μm in A (applies to A, E, I, M); 100 μm in B (applies to B-D, F-H, J-L, N-P).

Fig. S16. Kinesin-dependent localization of Reln protein.

(A-F) Reln protein and granule cell (GC) axons. 5-dpf WT (A-C, *n*=4) and *kif5aa*$^{*162/*162}$ *; kif5ba*$^{ae12/ae12}$ double mutant (D-F, *n*=7) larvae were stained with anti-Reln (magenta) and anti-Vglut1 (green) antibodies. Dorsal views with anterior to the left. Scale bars: 50 μm in A (applies to A-F). (G) The length and thickness of the Reln^{+} and Vglut1^{+} extra-cerebellar domains were measured and plotted. Both the length and the thickness of the Reln^{+} and Vglut1^{+} domains were significantly different in *kif5aa; kif5ba* mutants compared to WT (** $p<0.01$; *** $p<0.001$; Welch's *t* test for Reelin and Student's *t* test for Vglut1). Note that the granule cell axons were shorter, and Reln protein did not diffuse beyond the axons in the *kif5aa; kif5ba* mutant hindbrain.

Table

Table 1 Markers for the cerebellum and the cerebellum-like structures

Components	Markers	Marker types
(A) Cerebellum		
PC somata and neurites	parvalbumin7 (Pvalb7)	protein
	Tg(aldoca:gap43-Venus)	transgenic fish
PC somata	*grid2ipa*	mRNA
GC axons	Vglut1	protein
GC somata	Neurod1	protein
	vglut1	mRNA
GC axons and somata	hspGFFDMC90A;UAS:GFP	transgenic fish
CFs	calretinin	protein
	hspGFFDMC28C;UAS:GFP	transgenic fish
ECs	hspzGFFgDMC156A	transgenic fish
BGs	SAGFF(LF)251A;UAS:GFP	transgenic fish
(B) Mesencephalic tectum		
type I neurons	Pvalb7	protein
	grid2ipa	mRNA
type I neurons' somata	*pvalb7*	mRNA
GC axons	Vglut1	protein
GC somata	Neurod1	protein
	vglut1	mRNA
GC axons and somata	hspGFFDMC90A;UAS:GFP	transgenic fish

Signals of proteins and mRNAs were analyzed by immunohistochemistry and in situ hybridization, respectively. Expression of fluorescence proteins (Venus or GFP) in transgenic fish was examined to visualize neuronal or glial structure. Note that *vglut1* mRNA was localized in the GC somata whereas Vglut1 protein was localized in the GC axons in both cerebellum and mesencephalic tectum.

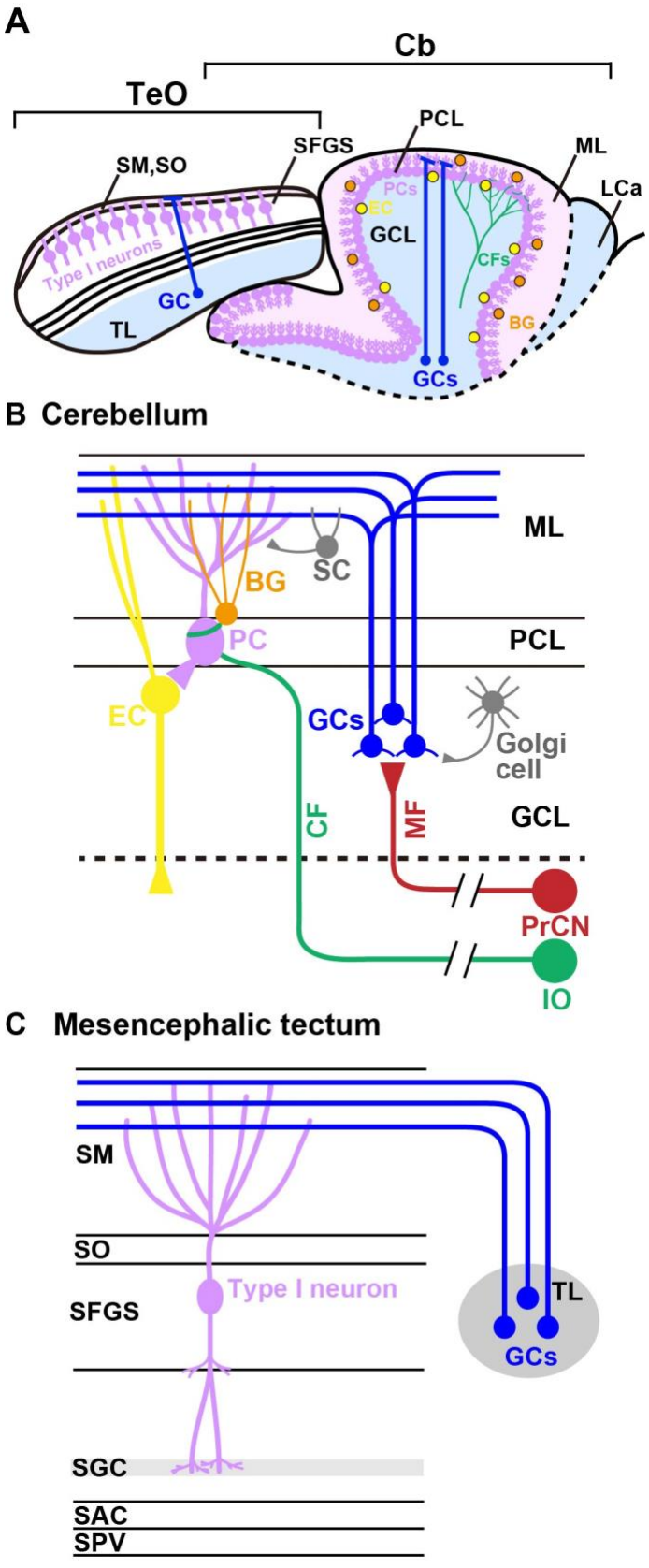

Fig. 1. Structure of cerebellum and mesencephalic tectum

Schematic presentation of zebrafish cerebellum, mesencephalic tectum, and neural circuits in these structures. (A) Sagittal section image of cerebellum and mesencephalic tectum. Neural circuits (transverse section images) in the cerebellum (B) and the cerebellum-like structure (C). BG, Bergmann glial cell; Cb, cerebellum; CF, climbing fiber; EC, eurydendroid cell; GC, granule cell; GCL, granule cell layer; IO, inferior olivary nucleus; LCa, lobes caudalis cerebelli; MF, mossy fiber; ML, molecular layer; PC, Purkinje cell; PCL, Purkinje cell layer; PrCN: precerebellar nucleus; SAC, stratum album centrale; SC, stellate cell; SFGS, stratum fibrosum et griseum superficiale; SGC, stratum griseum centrale; SM, stratum marginale; SO, stratum opticum; SPV, stratum periventriculare; TeO, tectum opticum; TL, torus longitudinalis.

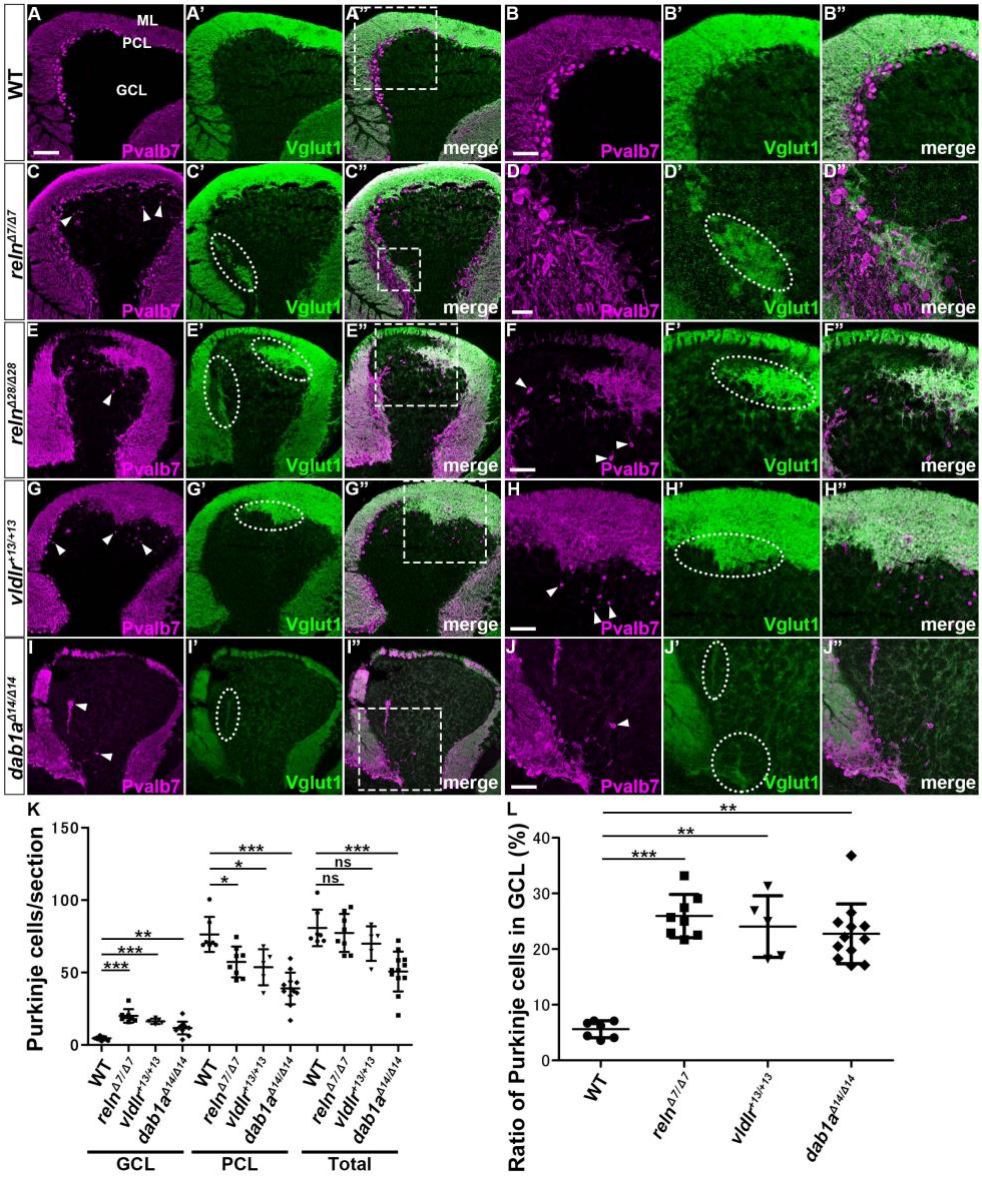

Fig. 2. Aberrant positioning of Purkinje cells (PCs) in adult zebrafish *reln*, *vldlr*, and *dab1a* mutants
(A-J) Sagittal sections of the brain from adult (90-150 dpf) wild-type (WT, A-A", *n*=6), and *reln* (C-C", E-E", *n*=5 for *reln*$^{\Delta7/\Delta7}$ and *n*=5 for *reln*$^{\Delta28/\Delta28}$), *vldlr*$^{+13/+13}$ (G-G", *n*=5), and *dab1a*$^{\Delta14/\Delta14}$ (I-I", *n*=8) mutant zebrafish were stained with anti-parvalbumin7 (Pvalb7, magenta) and anti-Vglut1 (green) antibodies. Typical cerebellum images are shown. (B-B", D-D", F-F", H-H", J-J") High magnification images of the boxes in A", C," E", G, and I". Ectopic Purkinje cells (PCs) are indicated by arrowheads. Axonal projections of granule cells (GCs) to ectopic PCs are marked by dotted circles. (K) Ectopic PCs. Sagittal sections 14-µm thick were prepared from adult zebrafish WT (*n*=7), and *reln*$^{\Delta7/\Delta7}$ (*n*=8), *vldlr*$^{+13/+13}$ (*n*=5), and *dab1a*$^{\Delta14/\Delta14}$ (*n*=12) mutant brains. Pvalb7^{+} PCs in the granule cell layer (GCL) or the Purkinje cell layer (PCL) were counted in every fourth section (14 total sections near the midline of each fish). Average numbers and standard deviations of PCs in the GCL, PCL, or all layers (Total) are shown in the graph. (L) Proportion of PCs in the GCL in WT, and *reln*$^{\Delta7/\Delta7}$, *vldlr*$^{+13/+13}$, and *dab1a*$^{\Delta14/\Delta14}$ mutant cerebellum. A greater proportion of the total PCs were located in the GCL in the *reln*, *vldlr*, and *dab1a* mutants than in WT. * $p < 0.05$; ** $p < 0.01$; *** $p < 0.001$; ns not significant (Dunnett's test for K and Dunn's multiple comparison test for L). Scale bars: 100 µm in A (applies to A-A", C-C", E-E", G-G", I-I"); 50 µm in B, D, F, H, and J (applies to B-B", D-D", F-F", H-H" and J-J", respectively).

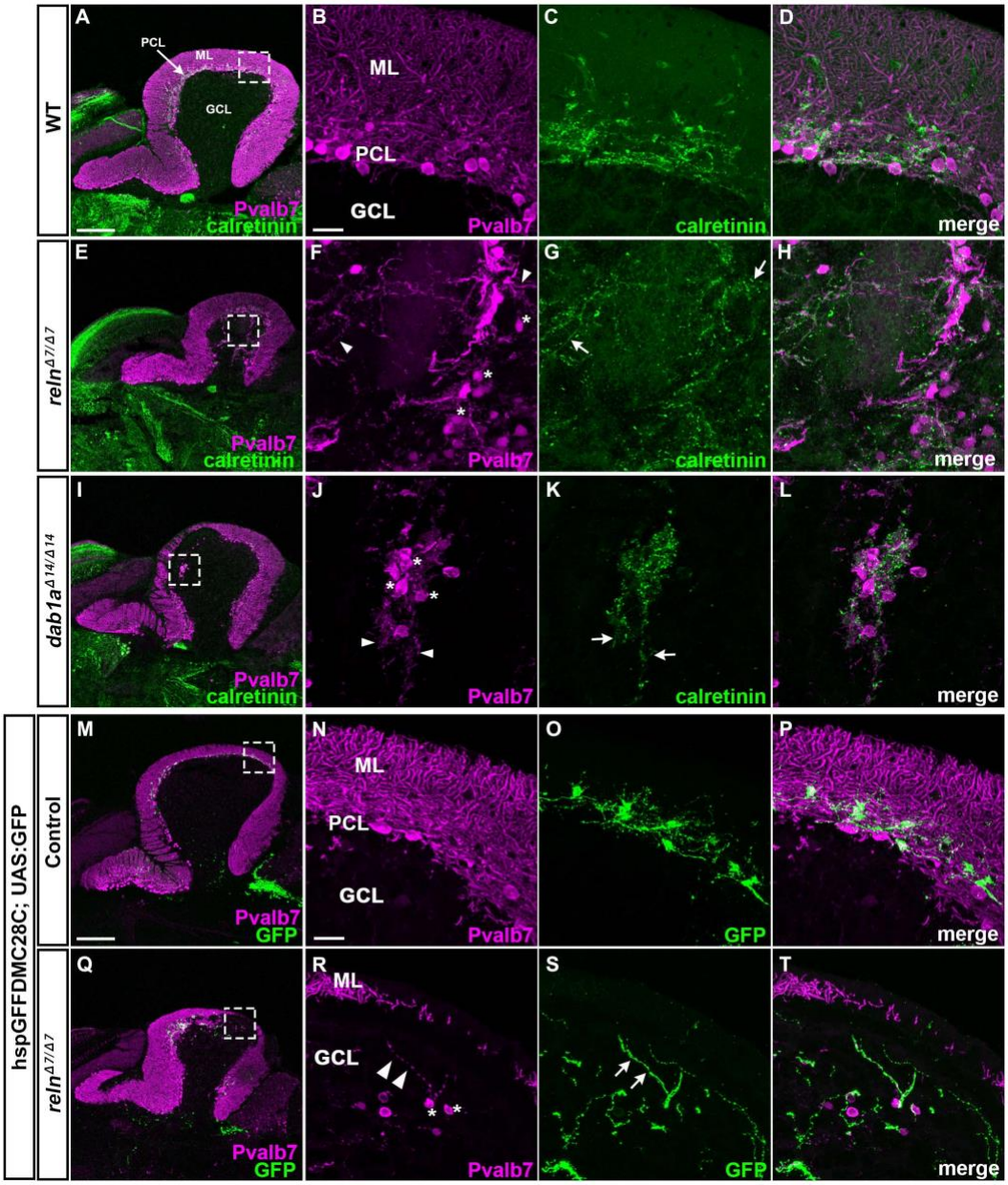

Fig. 3. Projection of climbing fibers (CFs) to ectopic PCs in *reln* and *dab1a* mutants
(A-L) Calretinin-immunoreactive (CR-ir+) axonal projections to PCs. Sagittal sections of adult (92-dpf) WT (A-D, *n*=4) and *reln*$^{\Delta 7/\Delta 7}$ mutant (E-L, *n*=4) brains were stained with anti-Pvalb7 (magenta) and anti-calretinin antibodies (green). (B-D, F-H, J-L) High magnification images of the boxes in A, E, and I. Typical images are shown. CR-ir+ axons projected to ectopic PCs located in the GCL in *reln* mutant cerebella, but not in WT cerebella. (M-T) CF projections to ectopic PCs. Sagittal section of adult (96 dpf) hspGFFDMC28C (28C); UAS:GFP fish brains, which express GFP in the CFs (axons of the neurons in the inferior olivary nuclei), harboring WT (control, *n*=4) or homozygous *reln* mutant (*reln*$^{\Delta 7/\Delta 7}$, *n*=4) alleles were stained with anti-Pvalb7 (magenta), and anti-GFP (green) antibodies. GFP+ CFs projected to ectopic PCs located in the GCL in *reln* mutant cerebella, but not in WT cerebella. Ectopic somata and dendrites of PCs are indicated by asterisks and arrowheads. CR-ir+ and 28C; UAS:GFP+ axons projecting to the ectopic Purkinje cells are indicated by arrows. The abbreviations are described in the legend for Fig. 1. Scale bars: 200 μm in A (applies to A, E, and I); 20 μm in B (applies to B-D, F-H, J-L); 200 μm in M (applies to M and Q); 20 μm in N (applies to R-T).

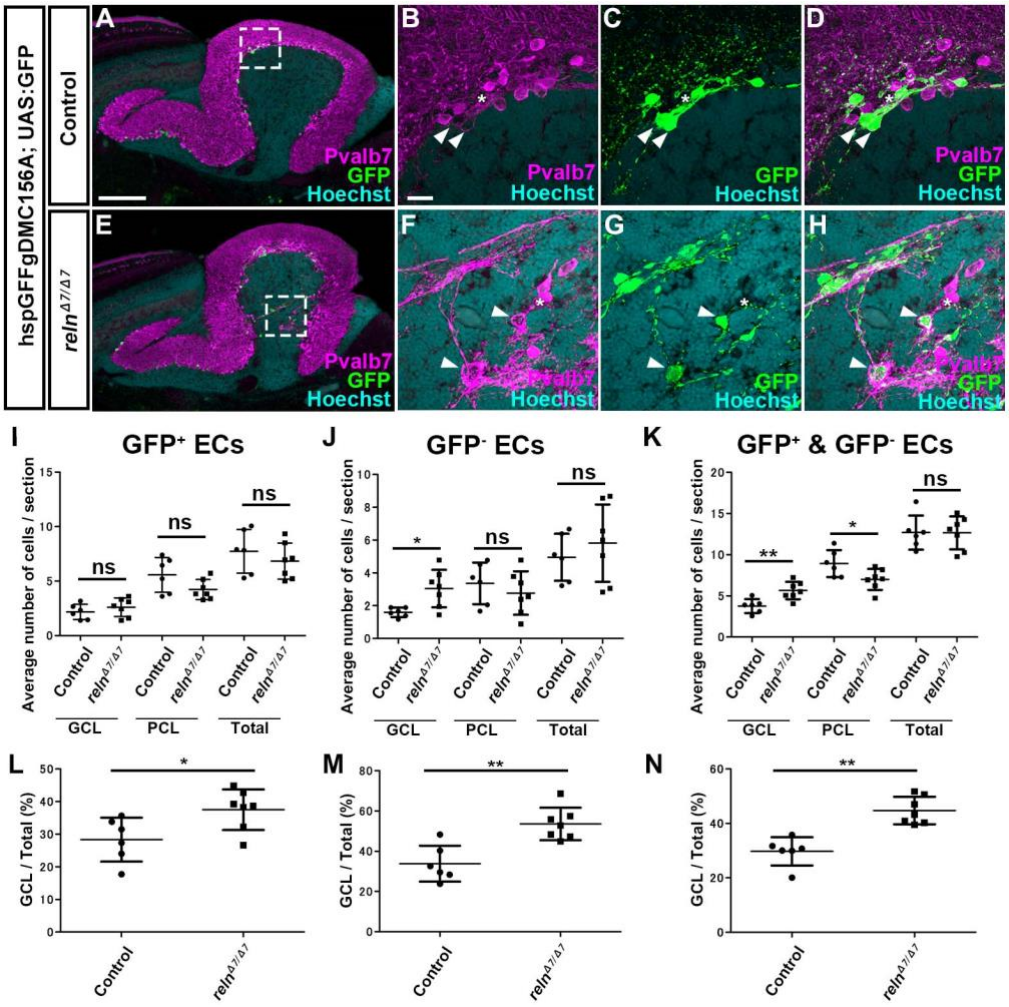

Fig. 4. Ectopic eurydendroid cells (ECs) in *reln* mutants

(A-H) Ectopic ECs in *reln*$^{Δ7/Δ7}$ mutants. Sagittal sections of adult (96-dpf) hspGFFgDMC156A; UAS:GFP zebrafish brains, which express GFP in ECs, harboring WT (control, *n*=6) or homozygous *reln* mutant (*reln*$^{Δ7/Δ7}$, *n*=7) alleles were stained with anti-Pvalb7 (magenta), anti-GFP (green) antibodies, and Hoechst (nucleus, cyan). (B-D, F-H) High magnification images of the boxes in A and E. There are two types of ECs: GFP^{+} (indicated by arrowheads) and GFP^{-} (asterisks) ECs, both of which receive the Pvalb7^{+} axons of PCs (somata are surrounded by Pvalb7^{+} axons). Ectopic GFP^{+} and GFP^{-} ECs were observed in the GCL of the *reln* mutant cerebellum (E-H). (I-K) GFP^{+} (I), GFP^{-} (J), and total (J) ECs in the GCL, the PCL, or all layers (Total) of the controls and *reln*$^{Δ7/Δ7}$ mutants were counted in every fourth section (18 total sections near the midline in each fish). Average numbers and standard deviations of ECs in the GCL, PCL, or all layers (Total) are shown in graphs. (L-N) Proportion of GFP^{+} (L), GFP^{-} (M), or total (N) ECs in the GCL in controls and *reln*$^{Δ7/Δ7}$ mutants. * $p < 0.05$; ** $p < 0.01$; ns not significant (Student's *t* test for J; Welch's *t* test for I and K; Mann-Whitney test for L-N). Scale bars: 200 μm in A (applies to A and E); 40 μm in B (applies to B-D, F-H).

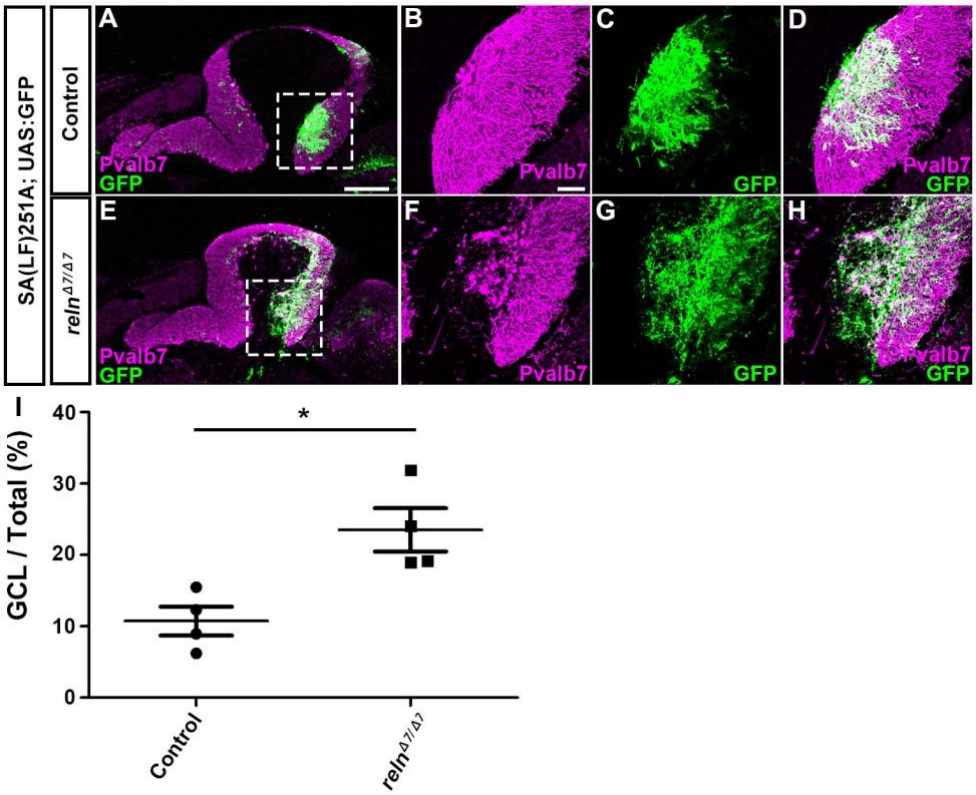

Fig. 5. Ectopic Bergmann glial cells (BGs) in *reln* mutants

(A-H) Aberrant localization of BGs in *reln* mutants. Sagittal section of adult (96 dpf) SAGFF(LF)251A; UAS:GFP brains, which express GFP in BGs, harboring WT (control, *n*=5) or homozygous *reln* mutant (*reln*$^{\Delta 7/\Delta 7}$, *n*=5) alleles were stained with anti-Pvalb7 (magenta) and anti-GFP (green) antibodies. (B-D, F-H) High magnification images of the boxes in A and E. (I) Ratio of the BG (GFP^{+}) area in the GCL to the total BG area in controls and *reln*$^{\Delta 7/\Delta 7}$ mutants. Fluorescence images were captured of every fourth section (16 total sections in each fish). The GFP^{+} area in the Pvalb7-negative GCL layer was measured and divided by the total GFP^{+} area in the cerebellum. * p <0.05 (Mann-Whitney U test). Scale bars: 300 μm in A (applies to E); 50 μm in B (applies to B-D and F-H).

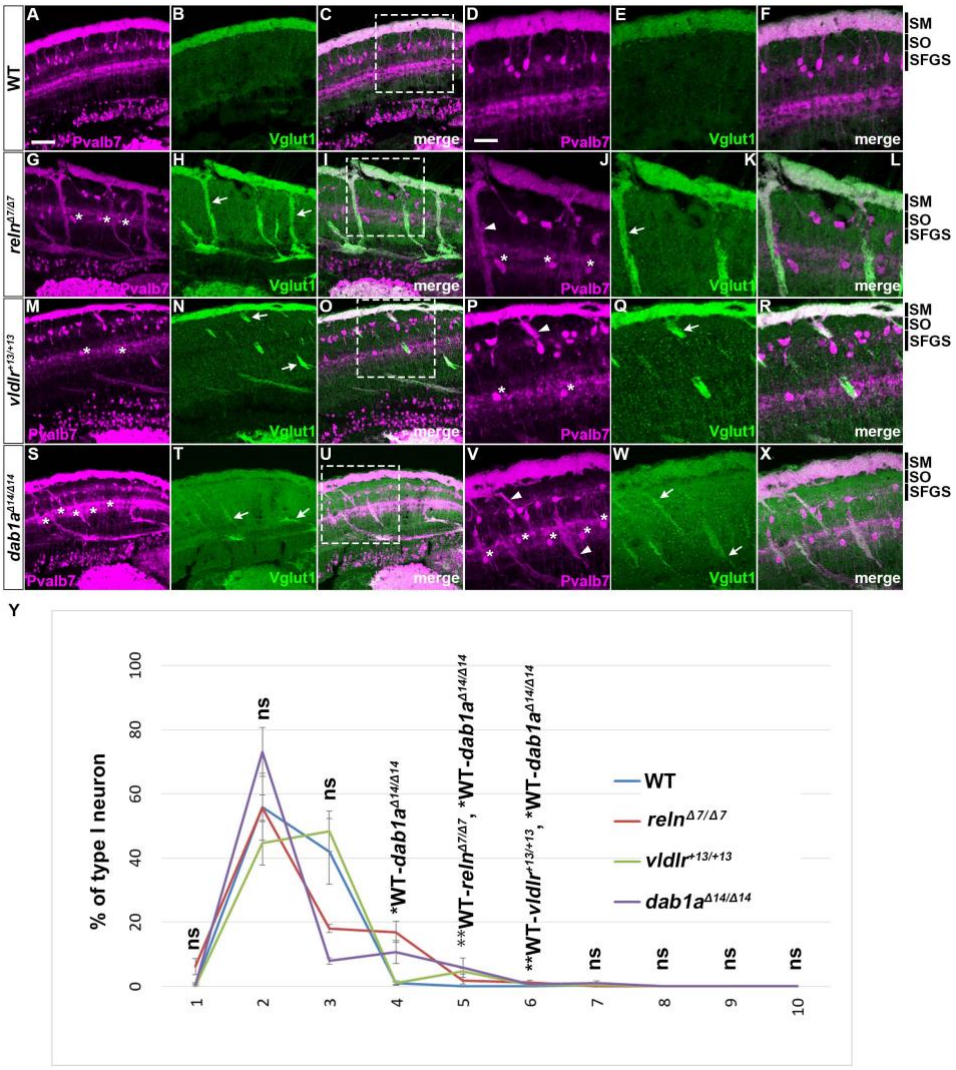

Fig. 6. Aberrant positioning of type I neurons in adult zebrafish *reln*, *vldlr*, and *dab1a* mutants
(A-X) Cross sections of the brain from adult (90-150 dpf) WT (A-F, *n*=9) and *reln*$^{\Delta 7/\Delta 7}$ (G-L, *n*=5), *vldlr*$^{+13/+13}$ (M-R, *n*=5), and *dab1a*$^{\Delta 14/\Delta 14}$ (S-X, *n*=4) mutant zebrafish were stained with anti- Pvalb7 (magenta) and anti-Vglut1 (green). Typical tectum images are shown. (D-F, J-L, P-R, V-X) High magnification images of the boxes in C, I, O, and U. Typical images are shown. Pvalb7^{+} type I neurons were located in a restricted area of the stratum fibrosum et griseum superficiale (SFGS) layer in the tectum in WT (A, D), but were ectopically localized in *reln*, *vldlr*, and *dab1a* mutants (indicated by asterisks in G, J, M, P, S, and V). Dendrites of some type I neurons were misoriented (indicated by arrowheads in J, P, and V). The Vglut1^{+} axons of granule cells (GCs) in the tectum project to dendrites of type I neurons in the stratum marginale (SM) in WT (B, E). These axons projected to ectopic type I neurons in *reln*, *vldlr*, and *dab1a* mutants (indicated by arrows in H, K, N, Q, T, and W). The stratum opticum (SO) is located between the SM and the SFGS. (Y) Position of type I neurons in WT (*n*=9), *reln*$^{\Delta 7/\Delta 7}$ (*n*=4), *vldlr*$^{+13/+13}$ (*n*=4), and *dab1a*$^{\Delta 14/\Delta 14}$ (*n*=4). The tectum region was divided into ten domains from the pia to ventricle. The positions of the type I neurons were determined by measuring the distance between the pia and the soma of type I neurons. Pvalb7^{+} cells located in the vicinity of the ventricular zone that had a morphology different from type I neurons were excluded. Average and standard deviation are indicated in the graph. * $p < 0.05$; ** $p < 0.01$; *** $p < 0.001$; ns not significant (Dunn's multiple comparison test). Scale bars: 20 μm in A (applies to A-C, G-I, M-O, and S-U); 40 μm in D (applies to D-F, J-L, P-R, and V-X).

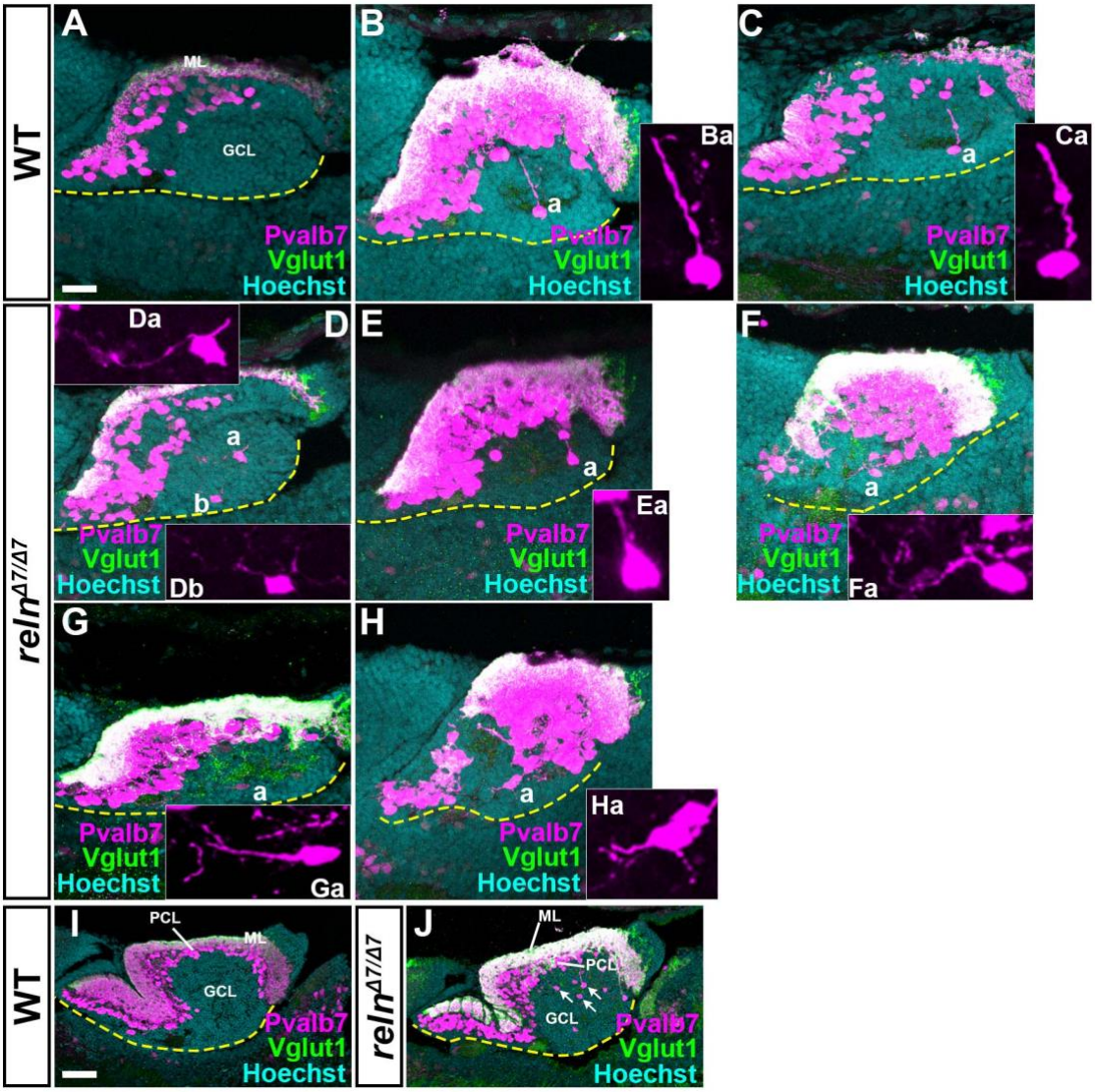

Fig. 7. Defects in the migration and polarity of PCs in *reln* mutants.
Sagittal sections of the brain from WT (A-C, *n*=4) and *reln*$^{\Delta7/\Delta7}$ (D-H, *n*=4) 15-dpf larvae, and from WT (I, *n*=3) and *reln*$^{\Delta7/\Delta7}$ (J, *n*=3) 30-dpf fish, were stained with anti-Pvalb7 (magenta) and anti-Vglut1 (green) antibodies, and Hoechst (cyan). Typical cerebellum images are shown. The ventral limit of the cerebellum is indicated by a dotted line. (Ba, Ca, Da, Ea, Fa, Ga, and Ha) High magnification images of the PCs marked by "a" in B-H. The Pvalb7 and Vglut1-double positive region marks the ML. Migrating PCs were detected in the GCL in WT, and they extended a neurite (primary dendrite) toward the pial side (Ba, Ca, *n*=4). Many of the migrating cells extended one or multiple neurites in aberrant directions in the *reln*$^{\Delta7/\Delta7}$ mutants (Ea, Fa, Ga, Ha, *n*=4). At 30 dpf, most of the PCs had reached the PCL in WT (I), whereas many ectopic PCs were detected in the GCL in *reln*$^{\Delta7/\Delta7}$ mutants (J, *n*=3). The abbreviations are described in the legend for Fig. 1. Scale bars: 20 μm in A (applies to A-H); 100 μm in I (applies to J).

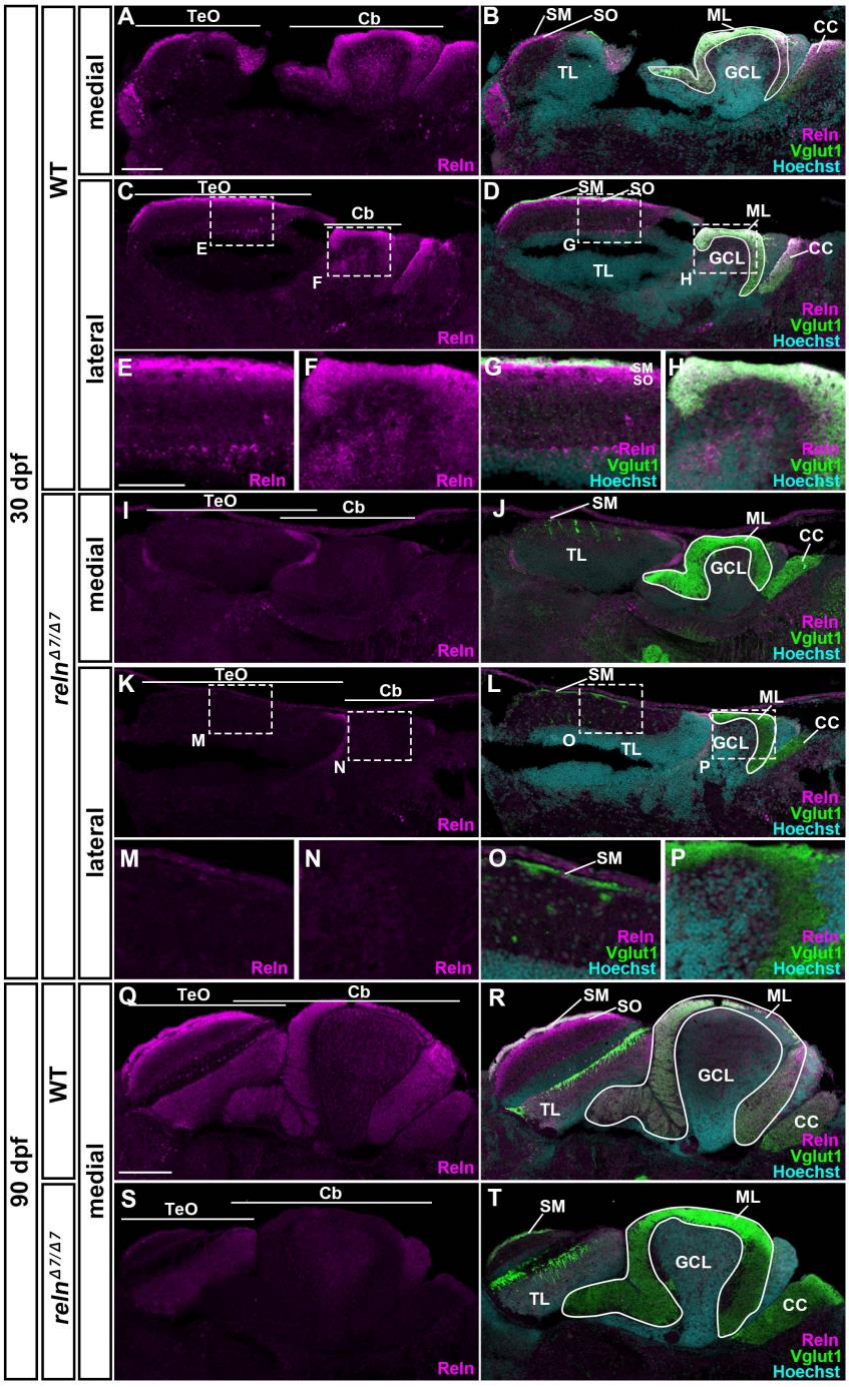

Fig. 8. Localization of Reln protein in the tectum and the cerebellum.
Medial and lateral sagittal sections of the brain from 30-dpf (A-P) and 90-dpf (Q-T) WT and *reln*$^{Δ7/Δ7}$ mutant zebrafish were stained with anti-Reln (magenta), anti-Vglut1 (green), and Hoechst (cyan). Three fish for 30-dpf and one fish for 90-dpf WT or *reln*$^{Δ7/Δ7}$ mutant fish were analyzed. Typical images are shown. (E-H, M-P) High magnification images of the boxes in C, D, K, and L. In WT, Reln protein was detected strongly in the SM and relatively weakly in the SO in the TeO. Reln was also detected strongly in the ML in the Cb. Weak Reln signals were also detected in the GCs in the TL and the GCL. These signals were absent in *reln*$^{Δ7/Δ7}$ mutants. CC, crista cerebellaris. The other abbreviations are described in the legend for Fig. 1. Scale bars: 100 μm in A (applies to A-D, I-L); 50 μm in E (applies to E-H, M-P); 200 μm in Q (applies to Q-T).

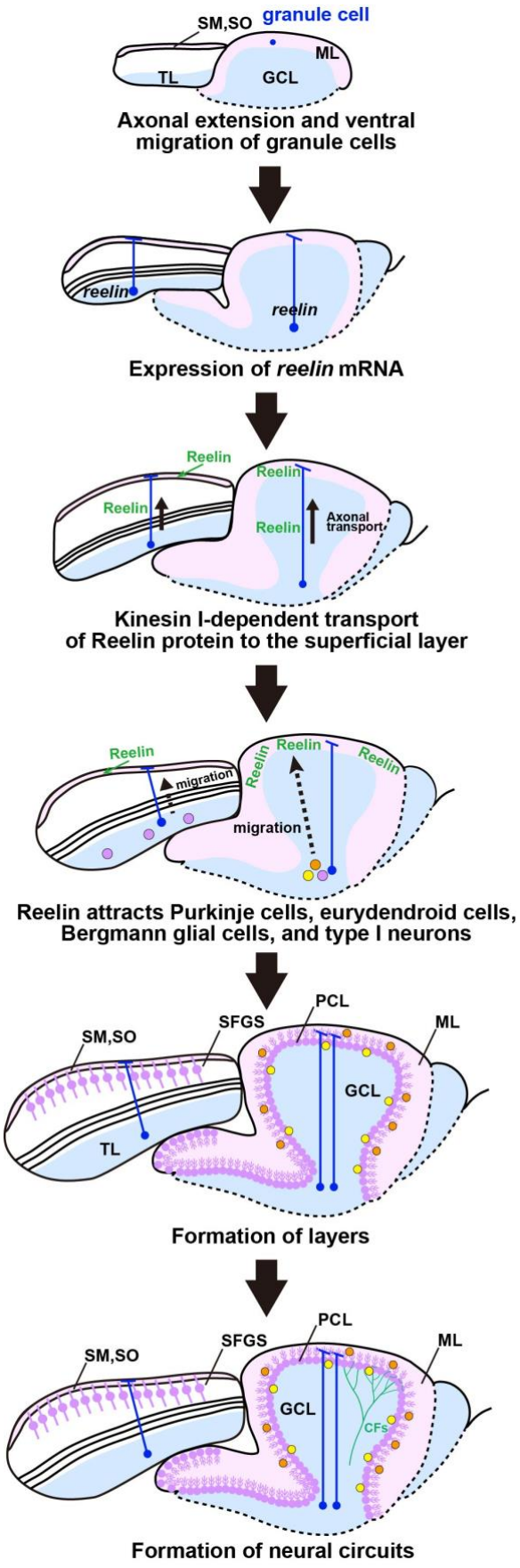

Fig. 9. Schematic diagram of the role of Reln signaling in the layer and neural circuit formation of the cerebellum and the mesecephalic tectum in zebrafish.
reln mRNA (*reelin*) and Reln protein (Reelin) are indicated by black and green letters, respectively. The somata of principal cells (PCs and type I neurons), BGs, and ECs are indicated by purple, orange, and yellow circles, respectively. Please see Discussion for details. The abbreviations are described in the legend for Fig. 1.

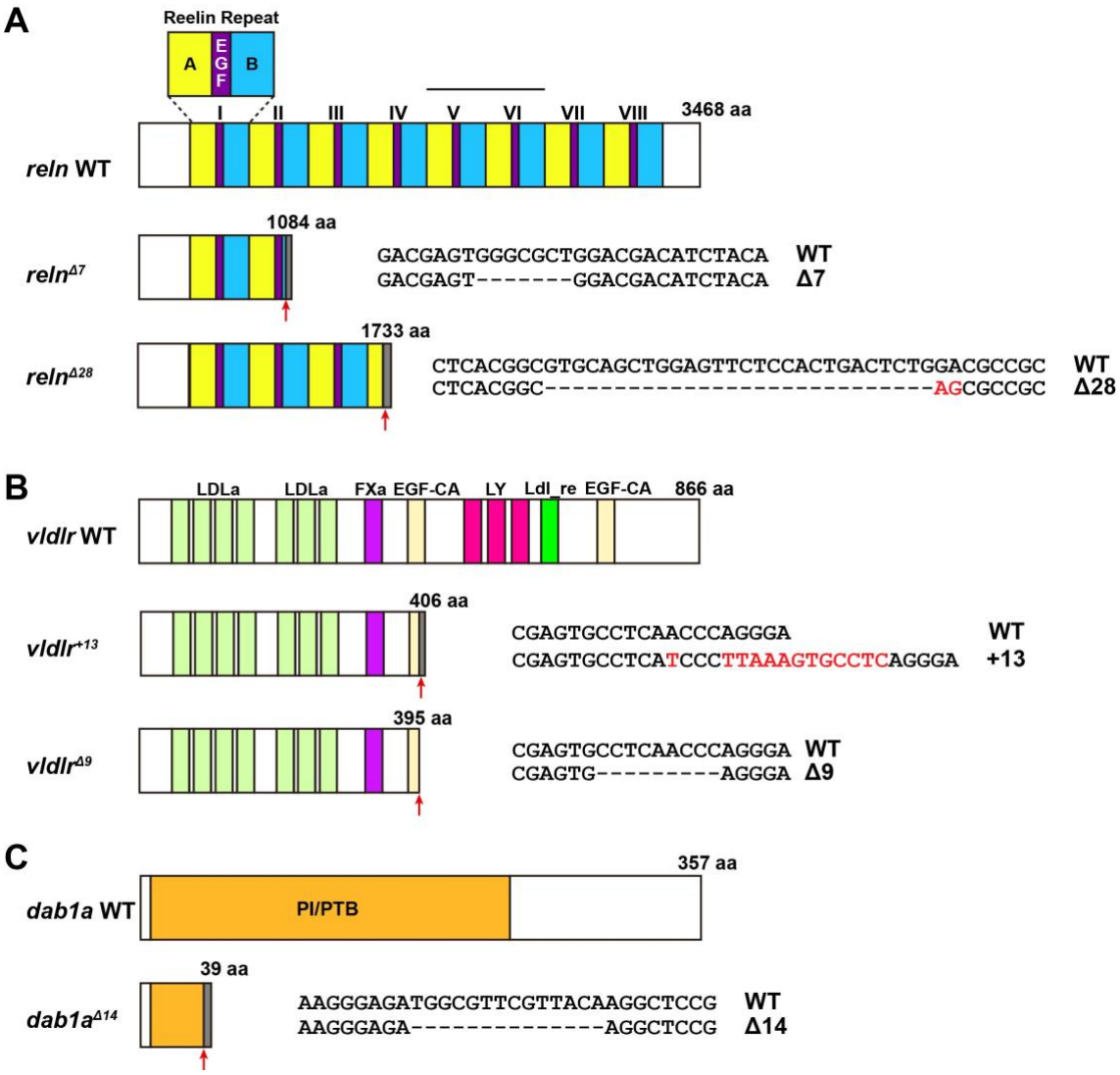

Fig. S1. Zebrafish *reln*, *vldlr*, and *dab1a* mutants.
Structure of wild-type and mutant Reln (A), Vldlr (B), and Dab1a (C). Reln has eight unique repeats (reelin repeats), each centered around an epidermal growth factor (EGF)-like cysteine pattern. A bar indicates the binding domain for the receptors (A). Vldlr has low-density lipoprotein receptor class A domains (LDLa), a coagulation factor Xa inhibitory site (FXa), calcium-binding EGF-like domains (EGF-CA), low-density lipoprotein-receptor YWTD domains (LY), and a low-density lipoprotein receptor repeat class B domain (Ldl_re) (B). Dab1a has a P-loop NTPase domain (Pl) and a phosphotyrosine-binding domain (PTB) (C). The nature of the mutations is also indicated. *reln*$^{\Delta 7}$ was established in this work. *reln*$^{\Delta 28}$, *vldlr*$^{+13}$, *vldlr*$^{\Delta 9}$, and *dab1a*$^{\Delta 14}$ were established previously (Di Donato et al., 2018). Red arrows indicate the positions corresponding to indel mutations. Red letters indicate inserted nucleotides. Amino acid numbers (aa) of the prospective wild-type and mutant proteins are indicated.

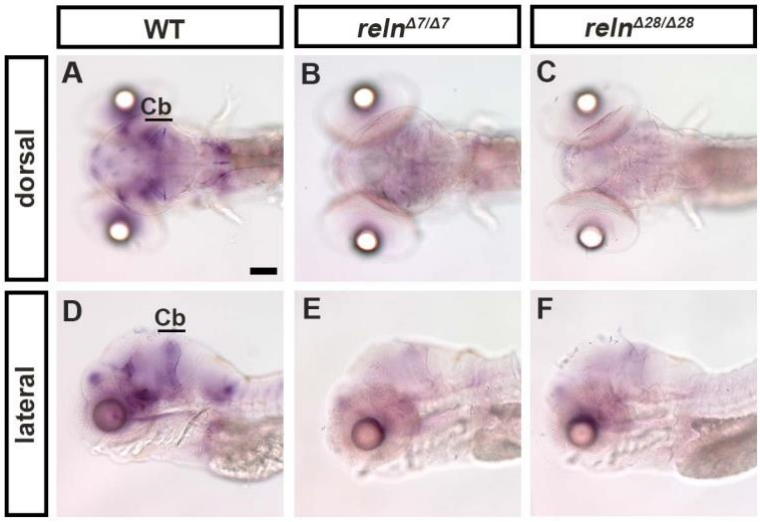

Fig. S2. *reln* transcripts are severely decreased in *reln* mutants.
Expression of *reln* in 5-dpf WT (A, D, *n*=2), *reln*$^{\Delta 7/\Delta 7}$ (B, E, *n*=2), and *reln*$^{\Delta 28/\Delta 28}$ (C, F, *n*=2) larvae was analyzed by whole-mount in situ hybridization. Note that the *reln* expression was severely decreased in the *reln* mutants. Cb, cerebellum. Scale bars: 100 μm in A.

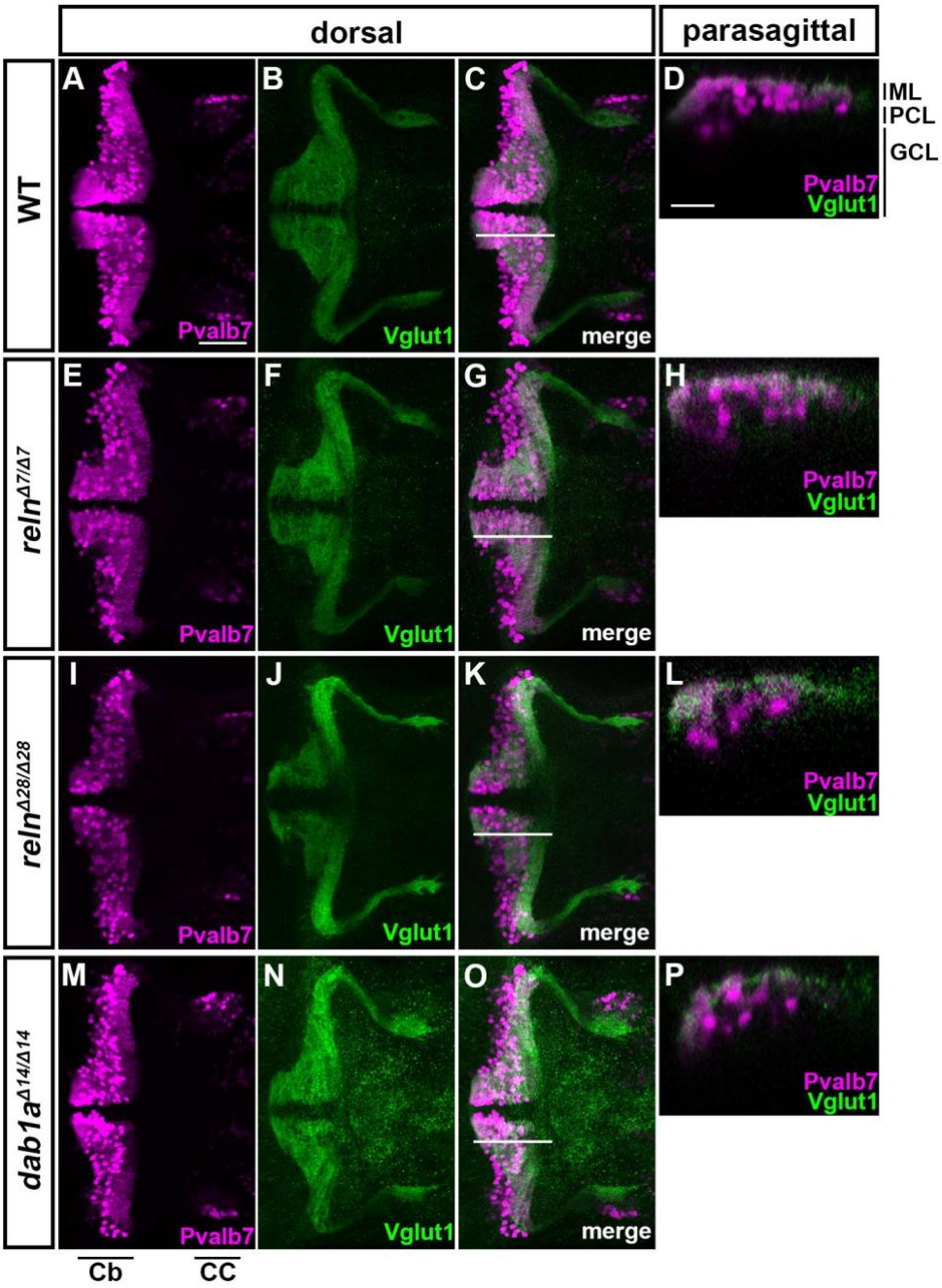

Fig. S3. Cerebellum development is not affected in *reln* or *dab1a* mutant early-stage larvae.
WT (A-D, *n*=8), *reln*$^{Δ7/Δ7}$ (E-H, *n*=5), *reln*$^{Δ28/Δ28}$ (I-L, *n*=9), and *dab1a*$^{Δ14/Δ14}$ (M-P, *n*=11) larvae at 5 dpf were stained with anti-Pvalb7 (magenta) and anti-Vglut1 (green) antibodies. Dorsal views with anterior to the left (A-C, E-G, I-K, M-O). Sagittal section images at the level indicated by lines in C, G, K, and O are shown in D, H, L, and P. Typical images are shown. Note that no abnormalities in the development of Pvalb7+ PCs or Vglut1+ GC axons or in the layer formation were observed in the *reln* and *dab1b* mutants. CC, crest cerebellaris. The other abbreviations are described in the legend of Fig. 1. Scale bars: 100 μm in A (applies to A-C, E-G, I-K, M-O); 20 μm in D (applies to D, H, L, P).

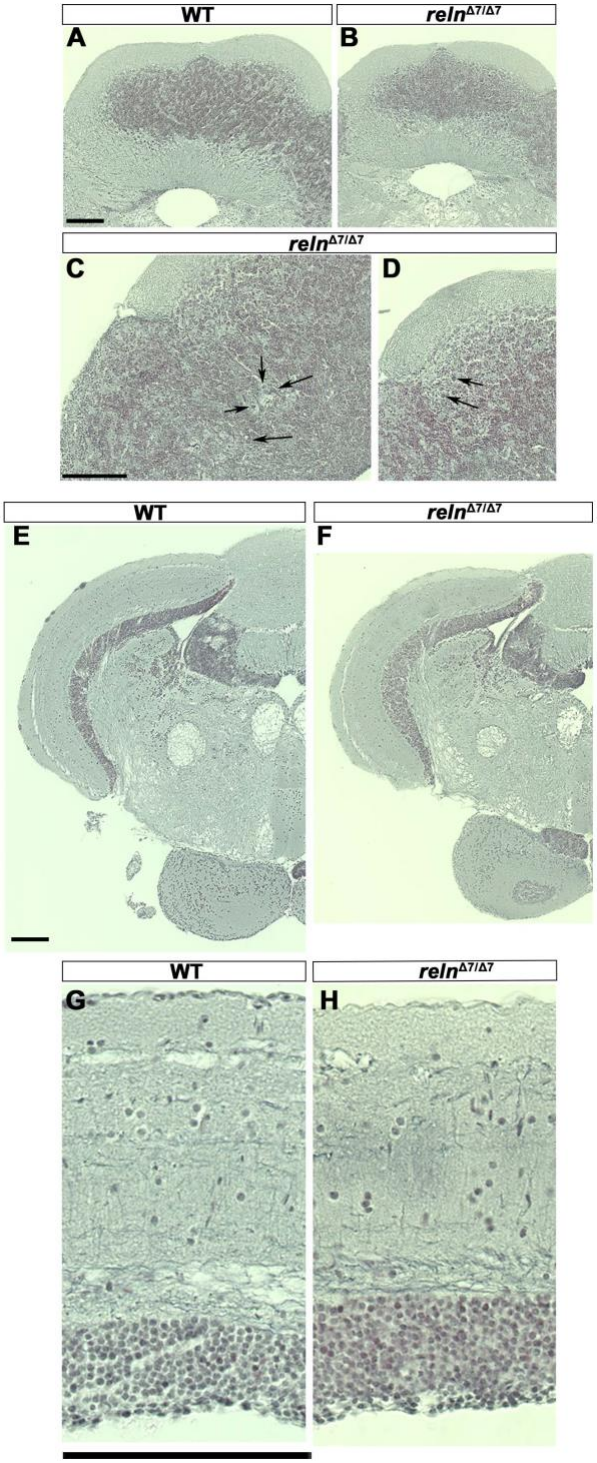

Fig. S4. Morphology of the cerebellum and the mesencephalic tectum in *reln* mutants.
Cross sections of the cerebellum (A-D) and the mesencephalon (E-H) of adult WT (A, E, G, *n*=2) and *reln*$_{\Delta 7/\Delta 7}$ mutant (B, C, D, F, and H, *n*=2) fish were stained by the Bodian silver impregnation method, which visualizes neuronal fibers (gray) and cell nuclei (purple). (C, D) High magnification images of the *reln*$_{\Delta 7/\Delta 7}$ mutant cerebellum. Arrows indicate ectopic neurons that have a large soma and are probably PCs in the GCL. (G, H) High magnification images of the WT and *reln*$_{\Delta 7/\Delta 7}$ mutant tectum. Note that no gross abnormalities in the tectum of the *reln* mutant were observed. Scale bars: 100 μm in A (applies to A, B); C (applies to C, D); E (applies to E, F); and G (applies to G, H).

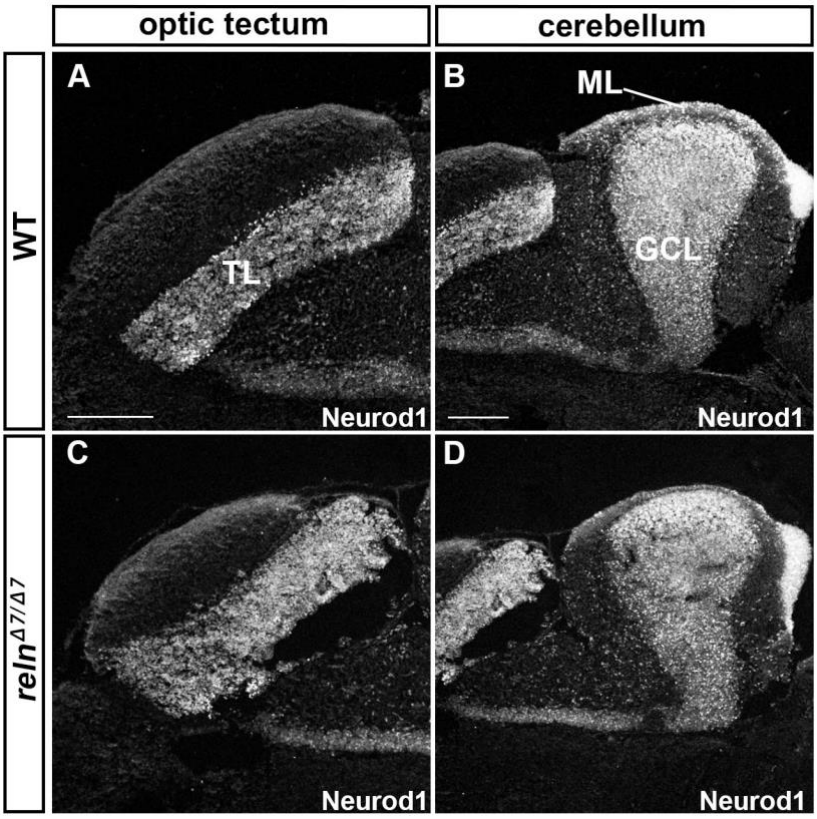

Fig. S5. Granule cell (GC) development is not affected in *reln* mutants.
Sagittal sections of the brain from adult (93-dpf) WT (A, B) and *reln*$^{Δ7/Δ7}$ (C, D) fish were stained with anti-Neurod1 antibodies, which mark the nucleus of immature and mature GCs in the TL, ML, and GCL. Note that the number and position of GC somata were largely unaffected in the *reln* mutants (*n*=6 for WT, and *n*=6 for *reln*$^{Δ7/Δ7}$ mutants). The abbreviations are described in the legend of Fig. 1. Sale bars: 100 μm in A (applies to A, C); 200 μm in B (applies to B, D).

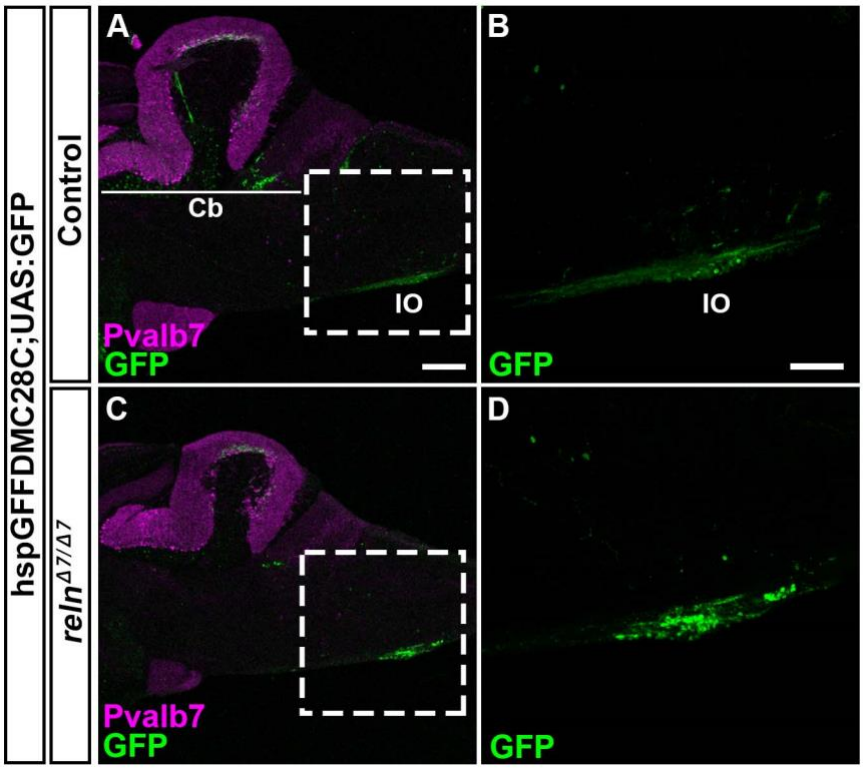

Fig. S6. Inferior olivary nuclei (IOs) are not affected in *reln* mutants.
Sagittal section of the brain from adult (90-150-dpf) control (A, B, *n*=4) and *reln*$^{\Delta 7/\Delta 7}$ mutant (C, D, *n*=4) fish with hspGFFDM28C; UAS:GFP, which marks the neurons in the IOs and their axons (CFs). (B, D) High magnification images of the boxes in A and C. Typical images are shown. Note that the number and position of the IO neurons were unaffected in the *reln* mutants. The abbreviations are described in the legend of Fig. 1. Scale bars: 40 μm in A (applies to A, C); 100 μm in B (applies to B, D).

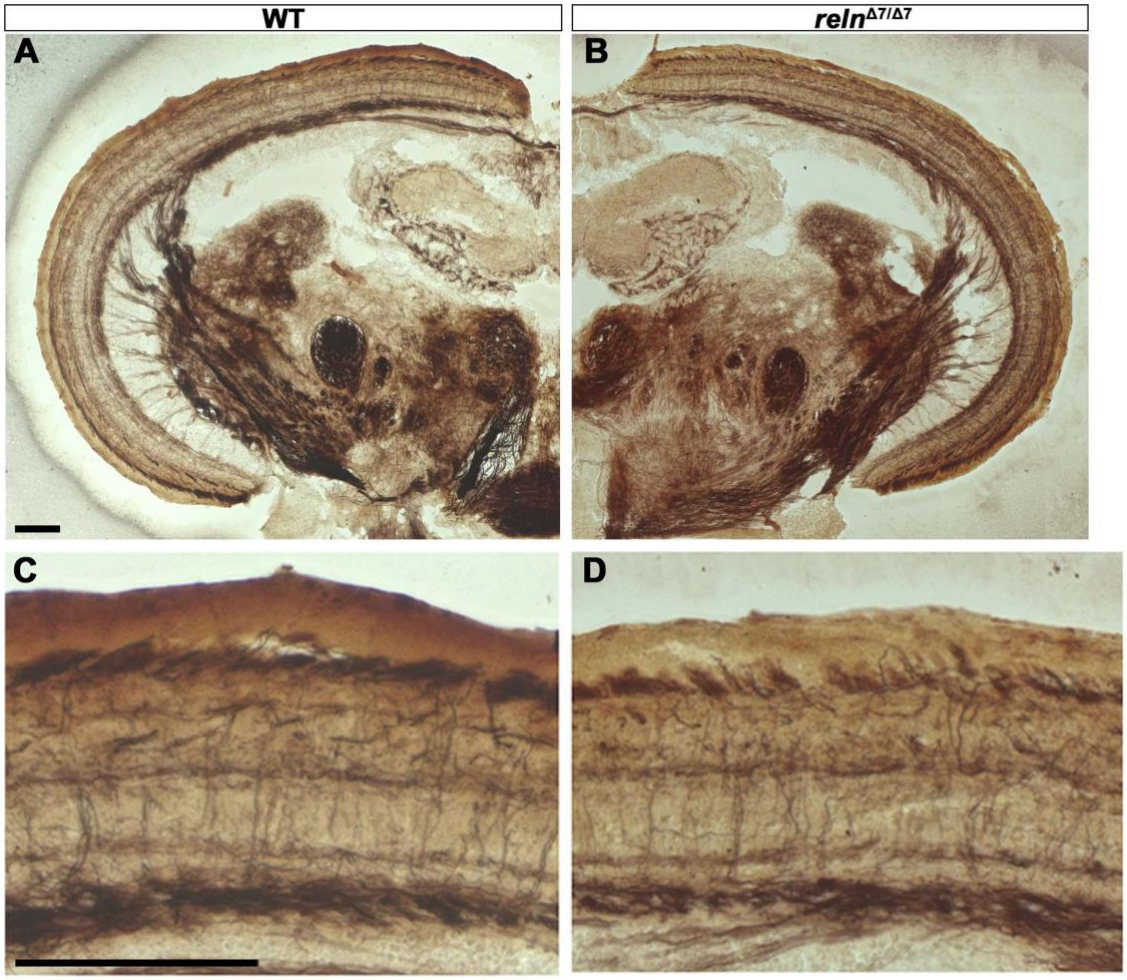

Fig. S7. Layer structure of the optic tecum is not affected in *reln* mutants.
Cross sections of the mesencephalon of adult WT (A, C, *n*=2) and *reln*$^{\Delta 7/\Delta 7}$ mutant (B, D, *n*=2) fish were stained by the Bielschowsky silver impregnation method, which visualizes neuronal fibers. (C, D) High magnification images of the tectum. Note that there was no difference in the neuronal fiber structure between the WT and the *reln* mutant tectum. Scale bars: 100 μm in A (applies to A, B) and C (applies to C, D).

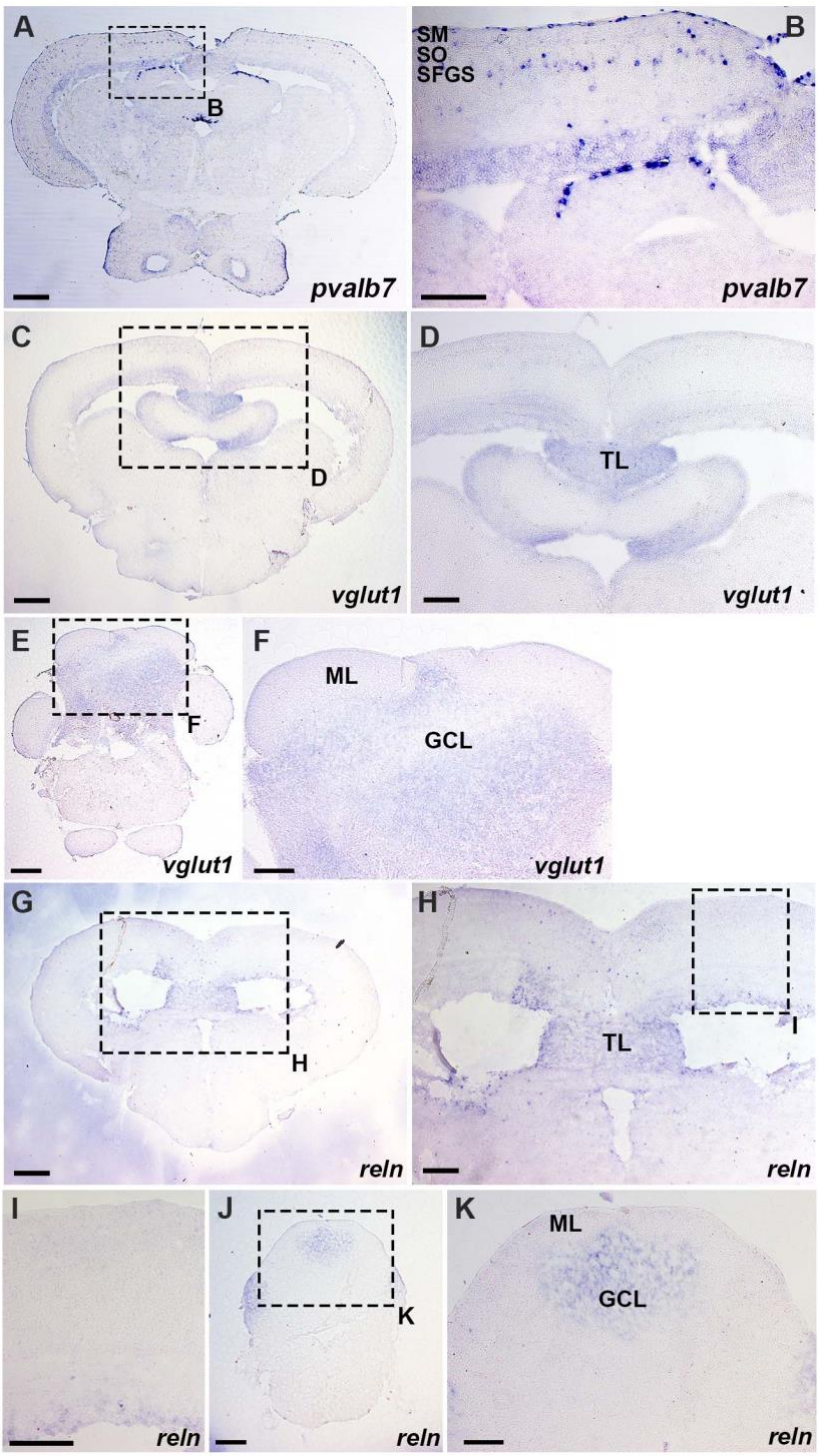

Fig. S8. Expression of *pvalb7*, *vglut1*, and *reln* in the mesencephalic tectum and the cerebellum. Cross sections of the mesencephalon (A-D, G-I) and the cerebellum (E, F, J, K) of adult WT zebrafish were stained with antisense riboprobes of *pvalb7* (A, B), *vglut1* (C-F), or *reln* (G-K) genes. (B, D, F, H, I, K) High magnification images of the boxes in A, C, E, G, H, and J. Note that *pvalb7*-expressing cells are located in the SFGS of the tectum (A, B), and *reln* and *vglut1* are not detected in the superficial layer of the tectum and the cerebellum (D, F, H, I). The abbreviations are described in the legend of Fig. 1. Scale bars: 200 μm in A, C, E, G, J; 100 μm in B, D, F, H, I, K.

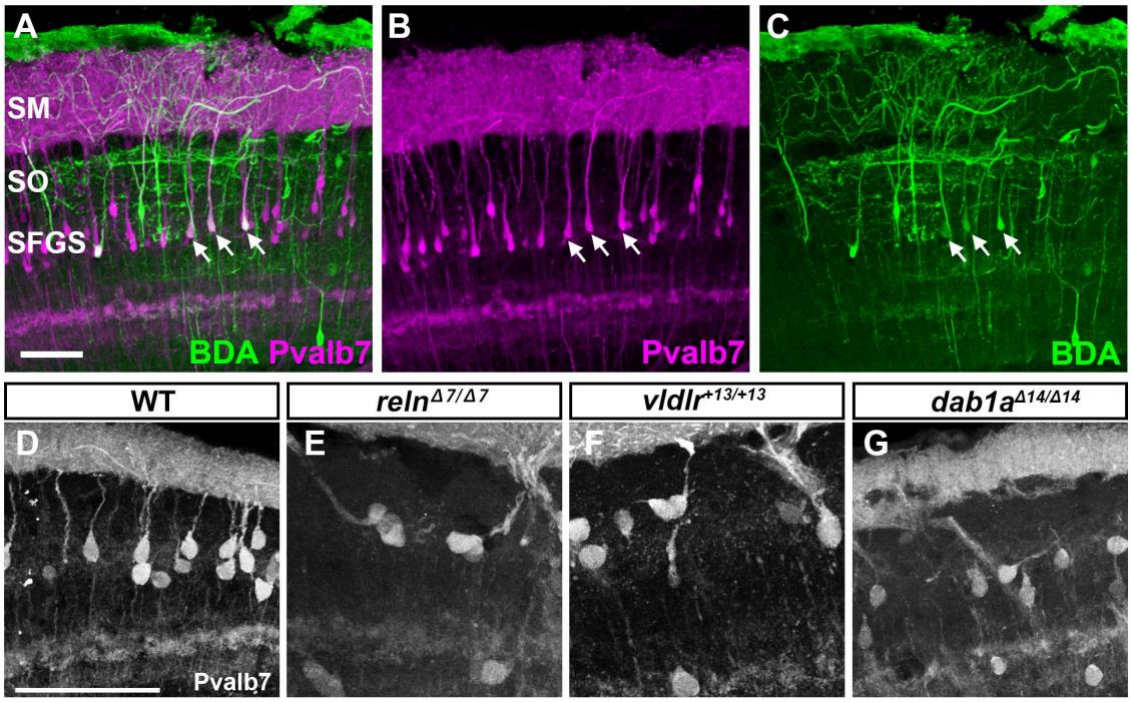

Fig. S9. Pvalb7 is a marker for type I neuron.
(A-C) Tracing of type I neurons. Biotinylated dextran amine (BDA) was injected into the SM of the tectum. After incubation, transverse sections were labeled with immunofluorescence using anti-Pvalb7 antibody (magenta) and fluorescent streptavidin (green). Note that the neurons labeled with BDA are also positive for Pvalb7 (indicated by arrows). (D-G) High magnification, grayscale images of Pvalb7-positive cells in Fig. 6D, J, P, and V. Scale bars: 50 μm in A (applies to A-C) and D (applies to D-G).

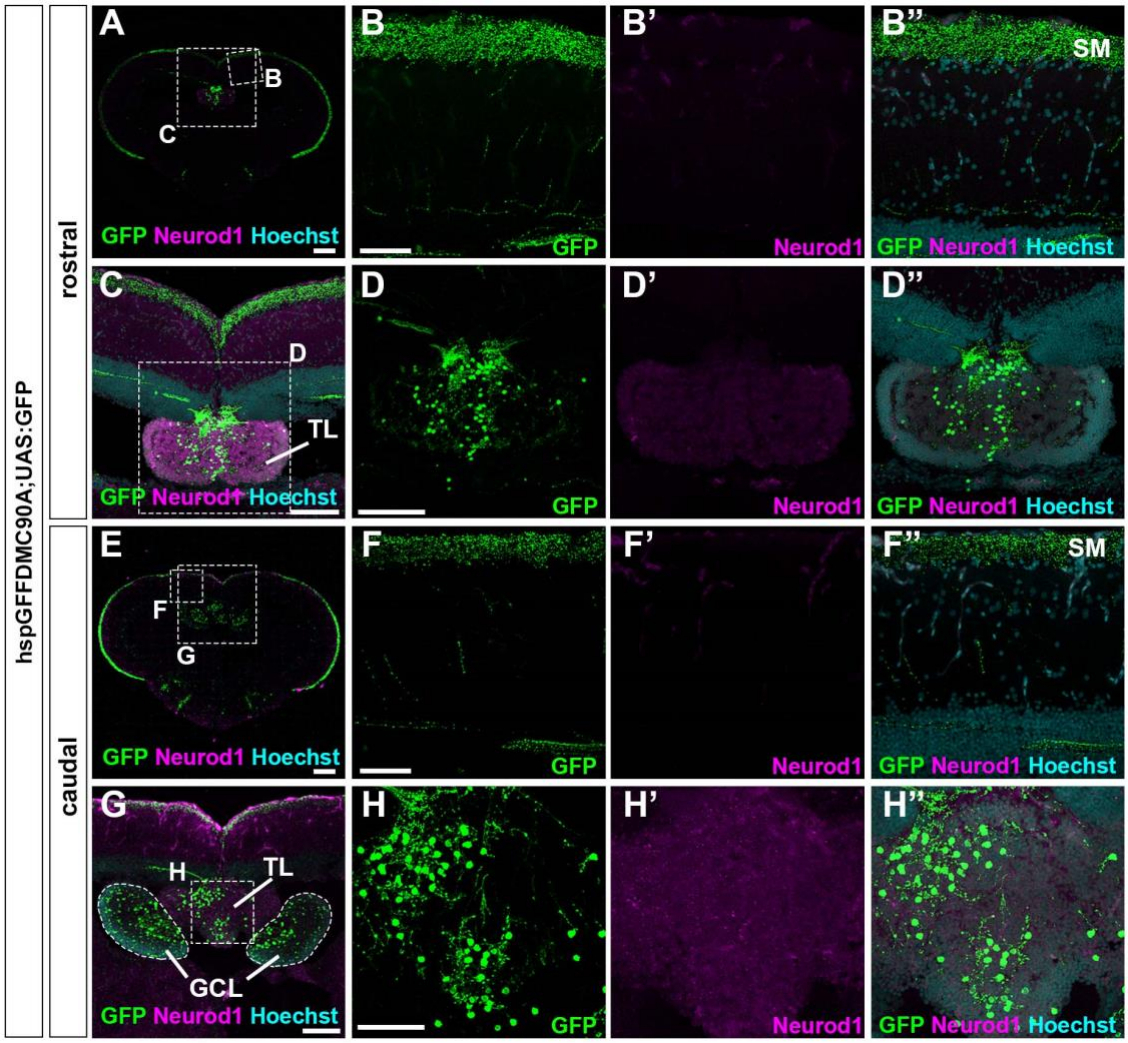

Fig. S10. Granule cells in the TL send their axons to the SM in the tectum.
Cross sections of a tectum region of the brain from adult hspGFFDMC90A;UAS:GFP fish, which express GFP specifically in GCs in the TL and the cerebellum, were stained with anti-GFP (green) and anti-Neurod1 (magenta) antibodies, and Hoechst (cyan). (B, C, D, F, G, H) High magnification images of the boxes in A, C, E, and G. Note that GFP was detected in the SM, the TL, and the GCL. The abbreviations are described in the legend of Fig. 1. Scale bars: 200 μm in A and E, 100 μm in C, D (applies to D', D"), and G, 50 μm in B (applies to B, B', B"); F (applies to F, F', F"); and H (applies to H, H', H").

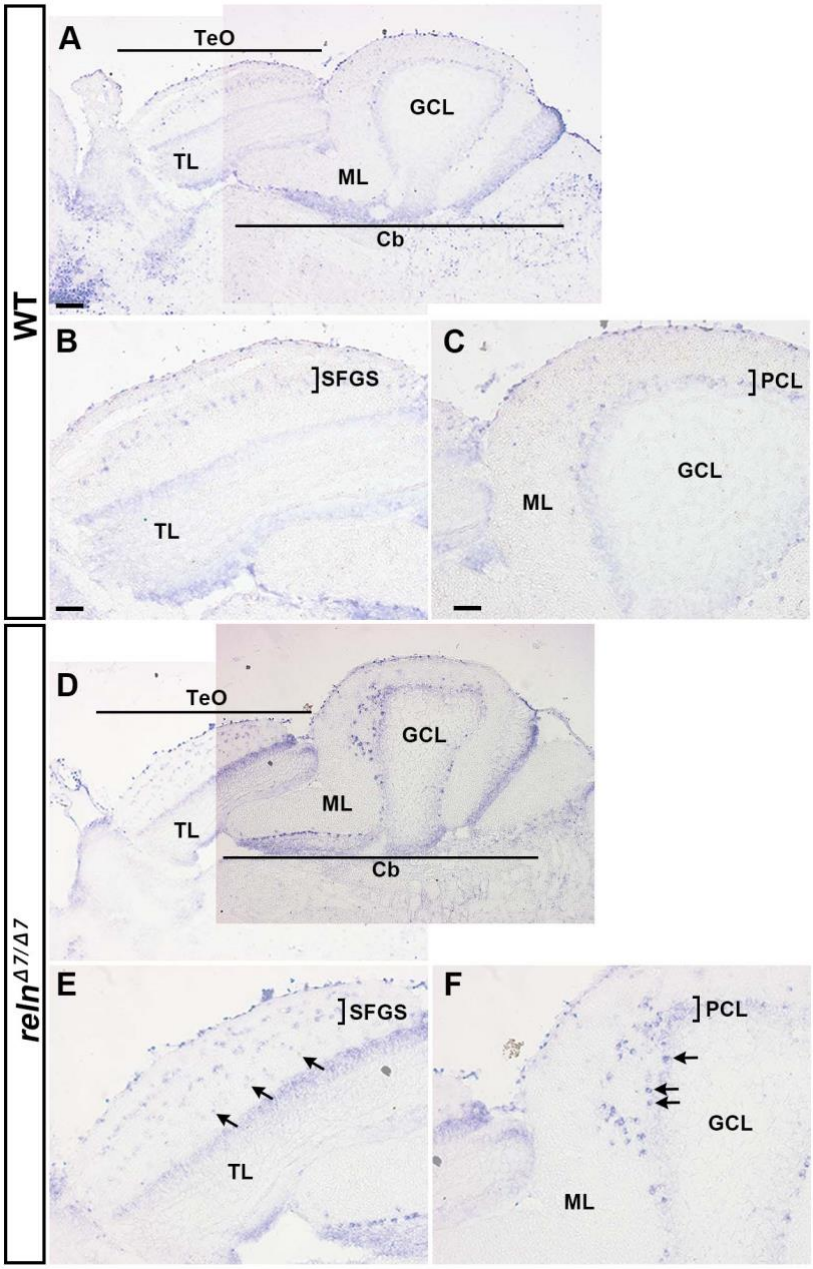

Fig. S11. Ectopic type I neurons and Purkinje cells (PCs) in *reln* mutants.
Sagittal sections from the brain of adult (159-dpf) WT (A-C, *n*=2) and *reln*$^{\Delta 7/\Delta 7}$ (D-F, *n*=2) zebrafish were stained with an antisense riboprobe for Grid2 interacting protein a (grid2ipa). *grid2ipa* transcripts were detected in type I neurons located in the SFGS of the TeO, and in PCs in the PCL of the Cb in WT. Ectopic *grid2ipa*-expressing type I neurons and PCs were observed in the *reln*$^{\Delta 7/\Delta 7}$ mutants (indicated by arrows). The abbreviations are described in the legend of Fig. 1. Scale bars: 100 μm in A (applies to A, D); 50 μm in B (applies to B, E); 50 μm in C (applies to C, F).

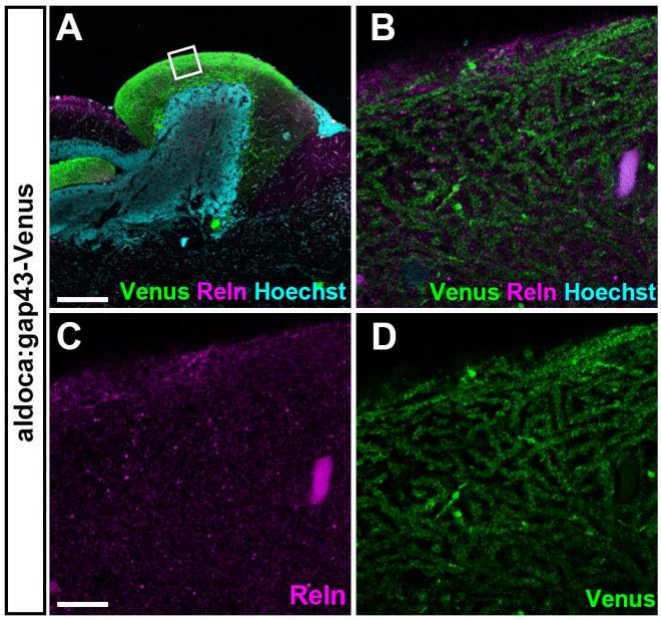

Fig. S12. Reln is not colocalized with dendrites of PCs in the ML of the cerebellum.
Sagittal sections of the brain from adult *Tg(aldoca:gap43-Venus)* fish, which express Venus in PCs, were stained with anti-GFP (Venus) and anti-Reln (magenta) antibodies, and Hoechst (cyan). Confocal optical sections (0.93 μm thickness). (B-D) High magnification images of the box in A. Note that Reln is not colocalized with PC dendrites. Scale bars: 200 μm in A; 10 μm in C (applies to B-D).

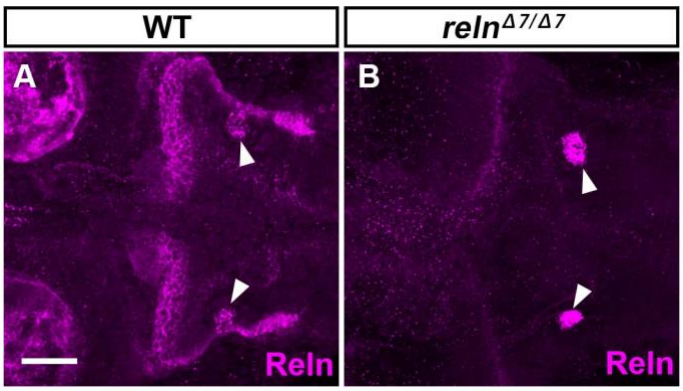

Fig. S13. Specific detection of Reln protein by immunostaining
WT (A, *n*=4) and *reln*$_{\Delta 7/\Delta 7}$ (B, *n*=3) larvae at 5-dpf were stained with anti-Reln (magenta) antibody. Dorsal views with anterior to the left. Typical images are shown. Note that Reln signals in and near the granule cell axons were severely decreased in the *reln* mutants. In some *reln* mutant larvae, nonspecific signals were also seen bilaterally in the hindbrain (marked by arrowheads). Scale bars: 100 μm in A.

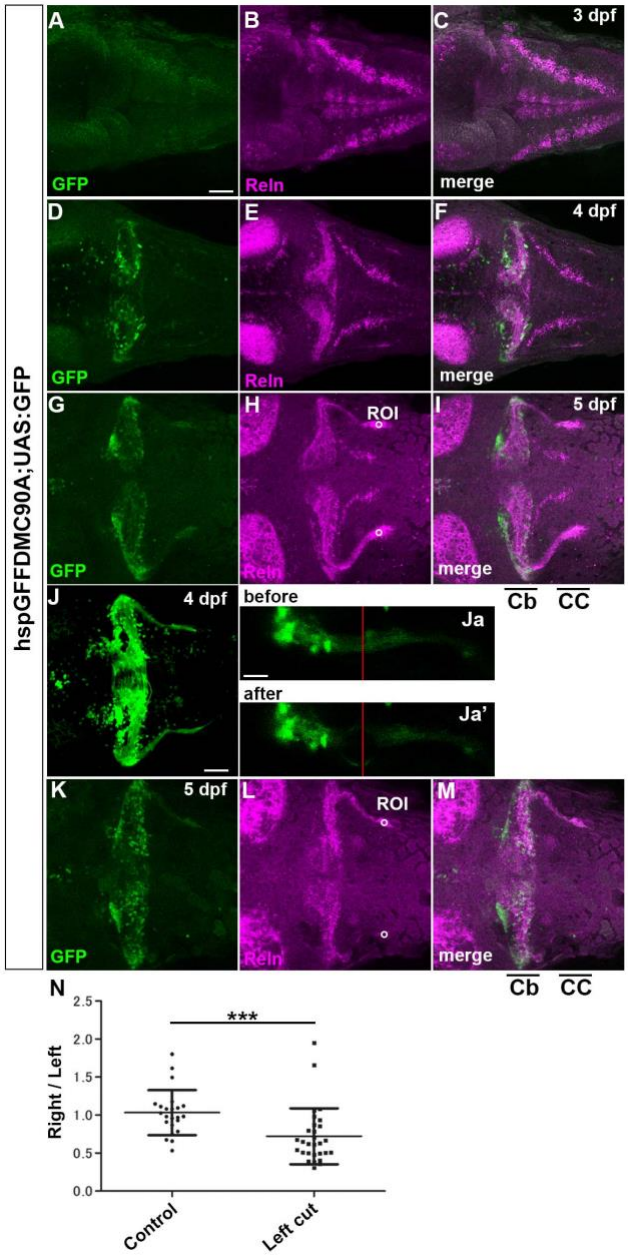

Fig. S14. Axon-dependent localization of Reln protein in GCs.

(A-I) GC axons and Reln localization. hspGFFDMC90A; UAS:GFP larvae, which express GFP in the soma and axons of GCs, were stained at 3-dpf (A-C), 4-dpf (D-F), and 5-dpf (G-I) with anti-GFP (green) and anti-Reln (magenta) antibodies. Typical data are shown. Reln was detected in or near GC axons in the cerebellum (Cb) and the crista cerebellaris (CC). (J, K) Ablation of GC axons. GC axons in the CC of 4-dpf hspGFFDMC90A; UAS:GFP larvae were ablated by a laser on the left side. (Ja, b) High magnification views of the left GC axons before (Ja) and after the ablation (Ja'). The point of the laser ablation is indicated by red lines. After the ablation, the larvae were reared and subjected to immunostaining with anti-GFP and anti-Reln antibodies at 5 dpf (K). Dorsal views with anterior to the left. Scale bars: 50 μm in A (applies to A-I, K-M); 50 μm in J; 20 μm (applies to Ja, Jb). (N) Fluorescence intensity of Reln signals on the right and left side (ROI, region of interest) in control (H, n=23) and laser-treated larvae (L, n=29) was measured. The ratio of the signal on the right to left side in each larva was calculated and plotted in a graph. The ratio was significantly different in the laser-treated larvae (*** p<0.001; Mann-Whitney test).

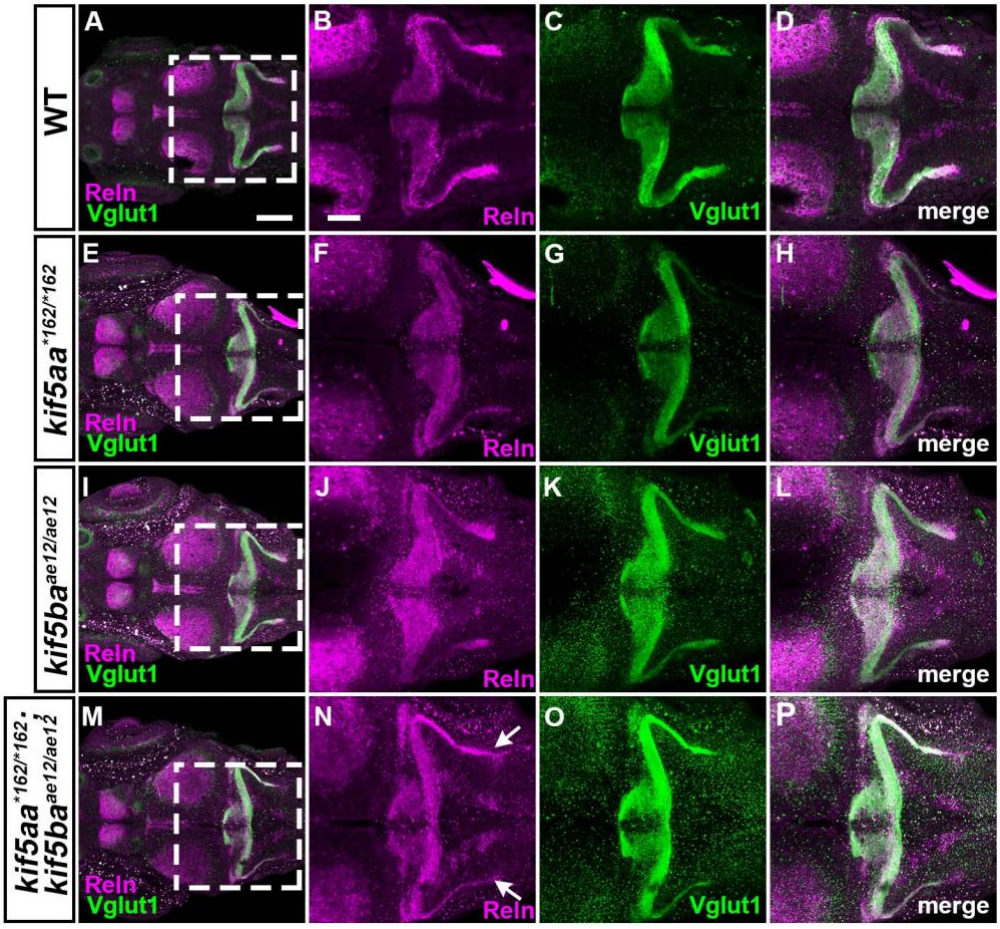

Fig. S15. Reln and GC axons in kinesin mutants.
WT (A-D, *n*=4), *kif5aa*$^{*162/*162}$ (E-H, *n*=13), *kif5ba*$^{ae12/ae12}$ (I-L, *n*=4), and *kif5aa*$^{*162/*162}$*; kif5ba*$^{ae12/ae12}$ (M-P, *n*=7) larvae at 5-dpf were stained with anti-Reln (magenta) and anti-Vglut1 (green) antibodies. Dorsal views with anterior to the left. (B-D, F-H, J-L, N-P) High magnification images of the boxes in A, E, I, and M. Typical images are shown. Note that the Reln and Vglut1 stainings were not strongly affected in the *kif5aa*$^{*162/*162}$ and *kif5ba*$^{ae12/ae12}$ single mutants, whereas they were decreased in the double mutants (indicated by arrows in N). Detailed analysis of the double mutants is shown in Fig. S1. Scale bars: 200 μm in A (applies to A, E, I, M); 100 μm in B (applies to B-D, F-H, J-L, N-P).

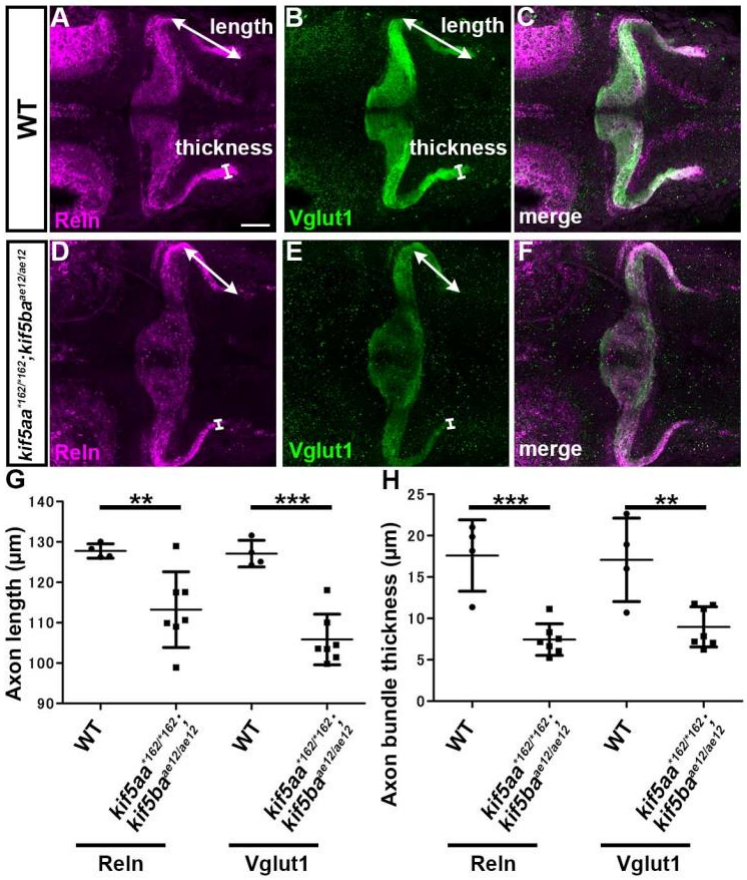

Fig. S16. Kinesin-dependent localization of Reln protein.
(A-F) Reln protein and granule cell (GC) axons. 5-dpf WT (A-C, *n*=4) and *kif5aa*$^{*162/*162}$ *; kif5ba*$^{ae12/ae12}$ double mutant (D-F, *n*=7) larvae were stained with anti-Reln (magenta) and anti-Vglut1 (green) antibodies. Dorsal views with anterior to the left. Scale bars: 50 µm in A (applies to A-F). (G) The length and thickness of the Reln+ and Vglut1+ extra-cerebellar domains were measured and plotted. Both the length and the thickness of the Reln+ and Vglut1+ domains were significantly different in *kif5aa; kif5ba* mutants compared to WT (** $p<0.01$; *** $p<0.001$; Welch's *t* test for Reelin and Student's *t* test for Vglut1). Note that the granule cell axons were shorter, and Reln protein did not diffuse beyond the axons in the *kif5aa; kif5ba* mutant hindbrain.